## Plant Physiology®

# An unexpected role for tomato threonine deaminase 2 in host defense against bacterial infection

In-Cheol Yeo  $\bigcirc$ , Ana Marcia Escocard de Azevedo Manhaes  $\bigcirc$ , Jun Liu  $\bigcirc$ , Julian Avila  $\bigcirc$ , Liu  $\bigcirc$ , Liu  $\bigcirc$ , Liu  $\bigcirc$ , Liu  $\bigcirc$ , Julian Avila  $\bigcirc$ , Liu  $\bigcirc$ ,

- 1 Department of Biochemistry and Biophysics, Texas A&M University, College Station, Texas 77843, USA
- \*Author for correspondence: tpd8@tamu.edu
- <sup>†</sup>Present address: Broad Institute, Cambridge, Massachusetts 02142, USA.

I-C.Y., J.A., and T.P.D. designed the research, I-C.Y., A.M.E.A.M., J.L., and J.A. performed the research, all authors analyzed data, I-C.Y. and T.P.D. wrote and revised the manuscript, and all authors read and commented on the manuscript.

The author responsible for distribution of materials integral to the findings presented in this article in accordance with the policy described in the Instructions for Authors (https://academic.oup.com/plphys/pages/General-Instructions) is Timothy P. Devarenne (tpd8@tamu.edu).

#### **Abstract**

Research Article

The hormones salicylic acid (SA) and jasmonic acid (JA) often act antagonistically in controlling plant defense pathways in response to hemibiotrophs/biotrophs (hemi/biotroph) and herbivores/necrotrophs, respectively. Threonine deaminase (TD) converts threonine to  $\alpha$ -ketobutyrate and ammonia as the committed step in isoleucine (IIe) biosynthesis and contributes to JA responses by producing the Ile needed to make the bioactive JA-Ile conjugate. Tomato (Solanum lycopersicum) plants have two TD genes: TD1 and TD2. A defensive role for TD2 against herbivores has been characterized in relation to JA-Ile production. However, it remains unknown whether TD2 is also involved in host defense against bacterial hemi/biotrophic and necrotrophic pathogens. Here, we show that in response to the bacterial pathogen-associated molecular pattern (PAMP) flagellin flg22 peptide, an activator of SA-based defense responses, TD2 activity is compromised, possibly through carboxy-terminal cleavage. TD2 knockdown (KD) plants showed increased resistance to the hemibiotrophic bacterial pathogen Pseudomonas syringae but were more susceptible to the necrotrophic fungal pathogen Botrytis cinerea, suggesting TD2 plays opposite roles in response to hemibiotrophic and necrotrophic pathogens. This TD2 KD plant differential response to different pathogens is consistent with SA- and JA-regulated defense gene expression. flg22-treated TD2 KD plants showed high expression levels of SA-responsive genes, whereas TD2 KD plants treated with the fungal PAMP chitin showed low expression levels of JA-responsive genes. This study indicates TD2 acts negatively in defense against hemibiotrophs and positively against necrotrophs and provides insight into a new TD2 function in the elaborate crosstalk between SA and JA signaling induced by pathogen infection.

### Introduction

In nature, plants are simultaneously faced with assault by numerous pathogens having different strategies for attacking hosts (Heil and Baldwin, 2002; de Souza et al., 2016). These plant pathogens are generally divided into biotrophs, hemibiotrophs, and necrotrophs based on their lifestyles for obtaining nutrients and water from a host plant (Glazebrook, 2005). Biotrophs require host plant tissues that are actively

metabolizing in order to obtain nutrients, thus the pathogen must keep the host alive (Reuber et al., 1998; Vogel and Somerville, 2000; Spanu and Panstruga, 2017). Hemibiotrophs first require living host tissue followed by a necrotic phase for nutrient access (Butt et al., 1998; Thaler et al., 2004). On the other hand, necrotrophs kill host cells by secreting degrading enzymes and toxin or effector molecules, which allow for access to nutrients from the dead tissues (Otani et al., 1998; MacKinnon et al.,

1999; Colmenares et al., 2002; Faris and Friesen, 2020). Therefore, plants possess elaborate molecular mechanisms that allow for efficient investment in and balance of the fitness costs needed for the inducible defense systems required to repel the various pathogens they encounter (Mur et al., 2006).

Plants have two levels of immunity: pattern-triggered immunity (PTI) and effector-triggered immunity (ETI). In PTI, conserved pathogen molecules termed pathogenassociated molecular patterns (PAMP), such as the flg22 peptide derived from bacterial flagellin and chitin from the fungal cell wall, are recognized through a series of cell surface pattern recognition receptors (PRR), which leads to the induction of basal defenses strong enough to defend against most pathogens (Jones and Dangl, 2006; Macho and Zipfel, 2014; Zipfel, 2014; Li et al., 2016). For ETI, pathogen produced effector proteins, with the purpose of suppressing PTI to cause disease, are recognized by host nucleotidebinding domain leucine-rich repeat (NLR) receptors. This leads to a strong defense response including the hypersensitive response, which involves the induction of host programmed cell death to kill the invading pathogen and prevent spread within the plant (Jones and Dangl, 2006; Cui et al., 2015).

Plant defense responses such as PTI are mediated by phytohormones. For example, salicylic acid (SA) controls resistance to hemibiotrophic/biotrophic (hemi/biotroph) pathogens, and jasmonic acid (JA) regulates defense responses to necrotrophic pathogens and insect herbivores (Glazebrook, 2005; Robert-Seilaniantz et al., 2011; Thaler et al., 2012). Because SA- and JA-mediated defense pathways target pathogens with different lifestyles, SA-JA crosstalk mostly results in reciprocal antagonism, i.e. SA responses suppress JA-mediated defenses and vice versa (Glazebrook, 2005; Robert-Seilaniantz et al., 2011; Pieterse et al., 2012; Thaler et al., 2012; Li et al., 2019; Yang et al., 2019). Accordingly, plants with mutations in SA signaling lose resistance to hemi/biotrophic pathogens while maintaining resistance to necrotrophic pathogens, and loss of JA signaling compromises defense against necrotrophs but leaves resistance to hemi/biotrophs intact (Thomma et al., 1998; Glazebrook, 2005). While it is well accepted that SA-JA signaling pathways are antagonistic, some studies have shown SA and JA responses act synergistically during defense (Schenk et al., 2000; van Wees et al., 2000; Mur et al., 2006; Truman et al., 2007; Liu et al., 2016).

During the development of these plant defensive traits individual genes have evolved to contribute to host defenses (Bergelson et al., 2001). One good example is tomato (Solanum lycopersicum) threonine deaminase 2 (TD2). Threonine deaminase (TD) is an enzyme that converts threonine to  $\alpha$ -ketobutyrate and ammonia (Supplemental Figure S1) as the committed step in the biosynthesis of isoleucine (Ile) in plants and microorganisms (Sidorov et al., 1981; Gallagher et al., 1998). In order for cells to maintain the proper concentration of Ile, TD activity is inhibited by

high concentrations of Ile interacting with the TD regulatory domain in a negative feedback regulation mechanism (Umbarger, 1956). Additionally, Ile-mediated inhibition of TD activity is partially restored in the presence of high concentrations of valine (Val; Supplemental Figure S1), the end product of a parallel competing pathway (Monod et al., 1965; Chen et al., 2013).

Most organisms have a single TD gene, however, tomato possesses two paralogous TD copies, TD1 and TD2. While TD1 fulfills a housekeeping function for Ile production, TD2 has a role in both Ile biosynthesis and a defensive role against herbivores (Chen et al., 2007; Gonzales-Vigil et al., 2011). In response to herbivore attack, TD2 expression is highly upregulated as a means to provide lle for the generation of the bioactive JA-Ile conjugate, which is the active form of JA for the induction of JA-mediated host defense responses (Kang et al., 2006). Moreover, tomato TD2 has a post-ingestive defensive role against herbivores, which directly disrupts the uptake of nutrients by the insect (Chen et al., 2005; Chen et al., 2007; Gonzales-Vigil et al., 2011). When tomato foliage is eaten by lepidopteran herbivores, TD2 is cleaved in the insect gut to generate a processed TD2 (pTD2), which results from proteolytic removal of the TD2 regulatory domain, thus removing any potential Ile-mediated inhibition (Gonzales-Vigil et al., 2011). In this form, pTD2 constitutively degrades Thr, eventually leading to nutritionally unbalanced proteins in the lepidopteran gut (Gonzales-Vigil et al., 2011). A role for tomato TD2 in the defense response against hemi/biotrophic bacterial pathogens has not been studied to date.

Recently, we serendipitously discovered that tomato TD2 is posttranslationally modified in response to treatment with the bacterial flg22 peptide using an antibody directed against a different protein. This modified TD2 shows increased sensitivity to Ile-feedback inhibition and flg22 treatment decreases TD2 enzyme activity in vivo. Using TD2 RNAi KD plants in defense assays suggest negative and positive roles for TD2 in resistance against hemi/biotrophic and necrotrophic pathogens, respectively. Based on these data, we propose a role for TD2 in contributing to the elaborate crosstalk between SA and JA responses.

#### Results

### An antibody raised against a tomato kinase transiently detects a different protein

The tomato Ser/Thr protein kinase Adi3 (AvrPto-dependent Pto-interacting protein 3) has cell death suppression (CDS) activity, and prevention of this CDS activity induces the cell death needed for resistance against the hemibiotrophic bacterial pathogen *Pseudomonas syringae* pv. *tomato* (*Pst*) during the ETI response (Devarenne et al., 2006; Ek-Ramos et al., 2010; Ek-Ramos et al., 2014). Phosphorylation of Adi3 by its upstream kinase, 3-phosphoinositide-dependent protein kinase-1 (Pdk1), is required for Adi3 CDS function (Devarenne et al., 2006; Ek-Ramos et al., 2010). In order to

study any possible role for Adi3 in the Pst-mediated PTI response, Adi3 phosphorylation dynamics in response to flg22 was analyzed using an Adi3 phosphospecific antibody (α-pAdi3) developed against a 15 amino acid phosphopeptide (Figure 1A). This  $\alpha$ -pAdi3 antibody was designed to detect the Pdk1-mediated Adi3 phosphorylation event at Ser539 (Figure 1A) (Devarenne et al., 2006), and by western blot (WB) showed specific detection of Pdk1 phosphorylated Adi3 from an in vitro kinase assay (Supplemental Figure S2). However, when tomato leaves were infiltrated with the flg22 peptide to induce the PTI response, the α-pAdi3 antibody instead detected a soluble protein by WB that had a lower molecular weight than the endogenous Adi3 (Figure 1B). Furthermore, this lower molecular weight protein displayed reduced detection by the  $\alpha$ -pAdi3 antibody in a time-depend manner in response to flg22 (Figure 1B). Over a 24-hour flg22 treatment, this decrease in protein detection by the  $\alpha$ -pAdi3 antibody was maintained for 50 minutes, by 1 hour after treatment the protein levels began to restore, and by 24 hours the protein was back to control levels (Figure 1C). These data indicate detection of this protein in response to flg22 is transient and can be restored to normal levels within 24 hours.

The simple explanation for these results is the  $\alpha$ -pAdi3 antibody detects a truncated version of Adi3, and Adi3 Ser539 phosphorylation is reduced in response to flg22. However, several lines of evidence suggest the  $\alpha$ -pAdi3 antibody detects a protein other than Adi3: (1) no full-length Adi3 is detected in the controls in Figure 1B; (2) Our previous studies (Ek-Ramos et al., 2010) have shown Adi3 protein is not degraded to smaller fragments; (3) Adi3 is found in the

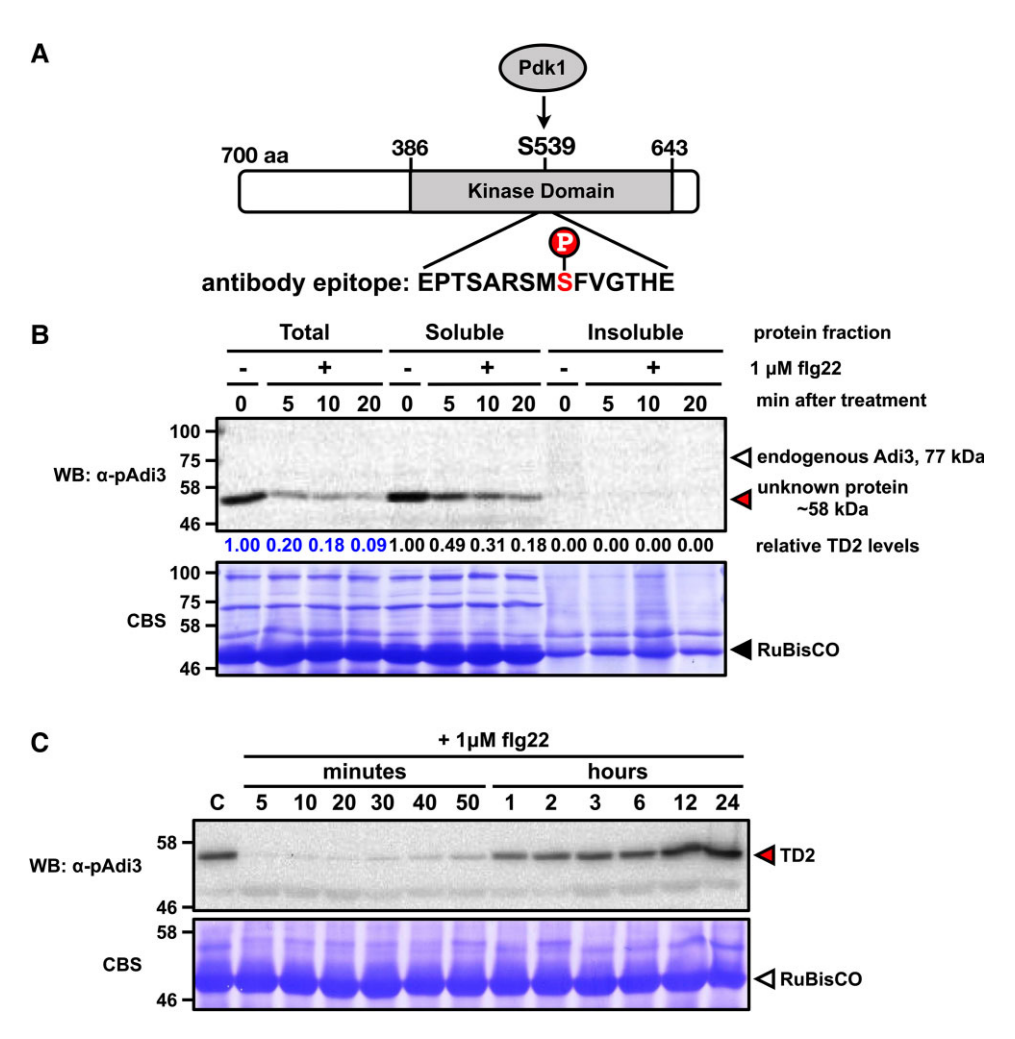


**Figure 1** Detection of a protein showing reduced detection by the  $\alpha$ -pAdi3 antibody in response to flg22 peptide treatment. A, Adi3 protein domains, Pdk1-mediated Ser539 phosphorylation site on Adi3, and sequence of the peptide used for producing the  $\alpha$ -pAdi3 antibody. B, Detection of an unknown protein by the  $\alpha$ -pAdi3 antibody in response to flg22. Tomato leaves were infiltrated with 1 μM flg22 and samples were collected at the indicated time points. 10 μg of total, soluble, and insoluble proteins were analyzed by  $\alpha$ -pAdi3 WB. C, Transient detection of the unknown protein by the  $\alpha$ -pAdi3 antibody in response to flg22. Tomato leaves were infiltrated with 1 μM flg22 and samples were collected at the indicated time points followed by  $\alpha$ -pAdi3 WB on 10 μg of soluble protein. In B and C, top panels, western blot (WB); bottom panels, Coomassie blue stain (CBS) of WB.

insoluble fraction of leaf extracts; and (4) Adi3 protein levels are tightly regulated and very low, suggesting the  $\alpha$ -pAdi3 antibody cannot detect endogenous Adi3 protein.

### Identification of threonine deaminase 2 and confirmation of its detection by the $\alpha$ -pAdi3 antibody

To identify the protein with compromised detection by the α-pAdi3 antibody in response to flg22 treatment, a 2D SDS-PAGE and mass spectrometry (MS) approach was performed with RuBisCO-depleted leaf extracts (Supplemental Figure S3A). A WB of the 2D SDS-PAGE analysis showed the protein detected by the  $\alpha$ -pAdi3 antibody was separated into several individual proteins indicating the target protein has different forms with distinct isoelectric point (pl) values (Supplemental Figure S3B). To identify this protein, the silver-stained proteins were excised for liquid chromatography-tandem mass spectrometry (LC-MS/MS) analysis (Supplemental Figure S3A). The results identified TD2 as the protein detected by the α-pAdi3 antibody from four independent analyses, and the best result showed 68.6% coverage of TD2 with 32 unique peptides excluding a chloroplast transit peptide (cTP) (Supplemental Figure S3C).

In order to support that TD2 is a bona fide target of the  $\alpha$ -pAdi3 antibody, the endogenous TD2 was immunoprecipitated from a leaf tissue extract using an  $\alpha$ -TD2 specific antibody (Chen et al., 2007) and then analyzed by WB using both the  $\alpha$ -TD2 and  $\alpha$ -pAdi3 antibodies. The results show the immunoprecipitated endogenous TD2 was detected by both

antibodies (Figure 2A). As mentioned above, tomato has two paralogous TD copies (Chen et al., 2007; Gonzales-Vigil et al., 2011). Although TD1 and TD2 do not share high amino acid identity with each other (51%; Supplemental Figure S4, A and B), it was necessary to test for detection of TD1 by the α-pAdi3 antibody. Thus, both recombinant, E. coli expressed, tomato 6xHis-TD1 and 6xHis-TD2 proteins were tested for WB detection by the  $\alpha$ -TD2 and  $\alpha$ -pAdi3 antibodies, and only the TD2 protein was detected by both antibodies (Figure 2B). This strongly indicates the α-pAdi3 antibody specifically detects the TD2 protein over the TD1 protein. Finally, a TD2 KD tomato line (Gonzales-Vigil et al., 2011) was utilized to verify TD2 detection by the  $\alpha$ -pAdi3 antibody. Although this TD2 KD plant was generated using the MicroTom cultivar, which is different from the Rio Grande PtoR cultivar we use as our research model, the TD2 proteins of the two cultivars share exactly the same amino acid sequence (Supplemental Figure S5). RuBisCOdepleted soluble protein extracts from leaves of PtoR WT, MicroTom WT, and MicroTom TD2 KD plants were analyzed by WB with the  $\alpha$ -TD2 and  $\alpha$ -pAdi3 antibodies. Both antibodies detected TD2 in the PtoR and MicroTom WT extracts, but TD2 was not detected in the MicroTom TD2 KD extract by either antibody (Figure 2C). Taken together, the  $\alpha$ -pAdi3 antibody detects the TD2 protein.

### Identification of the α-pAdi3 epitope in TD2

In an effort to find the TD2 epitope detected by the  $\alpha$ -pAdi3 antibody, several N- and C-terminally truncated versions

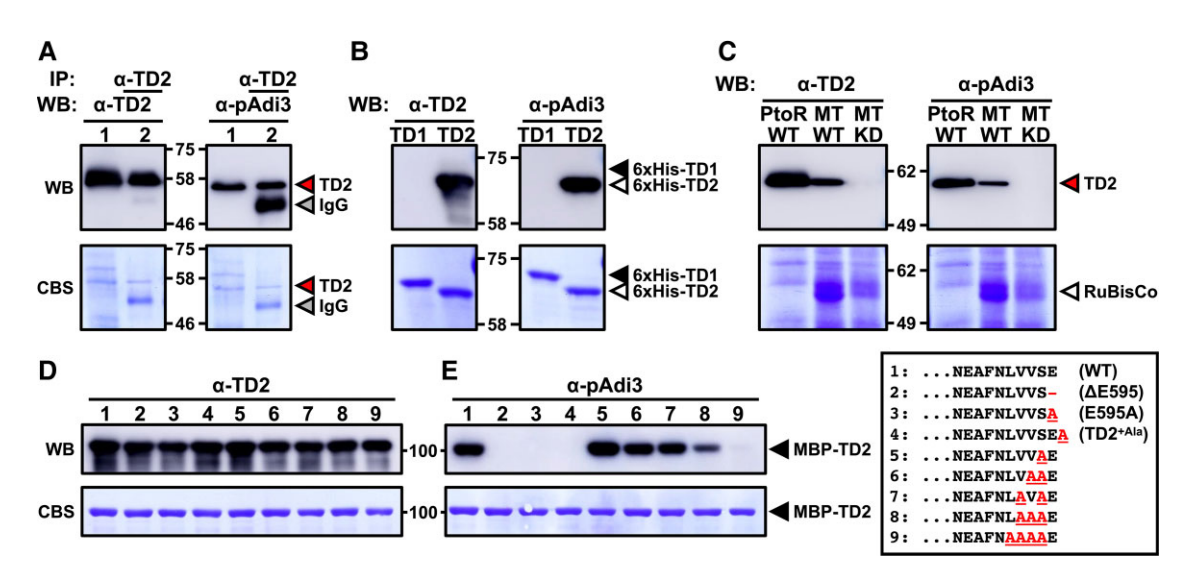


**Figure 2** Confirmation of TD2 detection by the α-pAdi3 antibody and TD2 epitope identification. A, The α-pAdi3 antibody detects TD2 protein immunoprecipitated (IP'd) by the α-TD2 antibody. Native TD2 protein was IP'd from leaf extracts using the α-TD2 antibody followed by WB with α-TD2 (left) and α-pAdi3 (right) antibodies. Lane 1, Soluble leaf proteins; lane 2, α-TD2 antibody IP'd proteins. IgG indicates rabbit IgG heavy chain from the α-TD2 antibody used for IP. B, the α-pAdi3 antibody detects TD2 and not TD1. Recombinant 6xHis-TD1 and 6xHis-TD2 proteins were analyzed by α-TD2 (left) and α-pAdi3 (right) WB. C, Loss of TD2 detection by the α-pAdi3 antibody in MicroTom (MT) TD2 knockdown (KD) plants. The RuBisCO-depleted soluble protein extracts from Rio Grande PtoR wild-type, MT, WT, and MT-TD2 knockdown (KD) plants were analyzed by α-TD2 (left) and α-pAdi3 (right) WB. D and E, Identification of the α-pAdi3 epitope in TD2. The recombinant MBP-TD2 point mutants shown in the box, mutations in red and underlined, were analyzed by α-TD2 (D) and α-pAdi3 (E) WB. For all panels, top panels, western blot (WB); bottom panels, Coomassie blue stain (CBS) of WB.

of the recombinant MBP-TD2 protein were tested. Four N-terminally truncated TD2 proteins were generated (Supplemental Figure S6A) and analyzed by  $\alpha$ -TD2 and α-pAdi3 WB (Supplemental Figure S6B). Detection of all N-terminally truncated TD2 versions by both antibodies was confirmed (Supplemental Figure S6B, lanes 3-6). The shortest N-terminally truncated TD2 protein contained only the last 94 amino acids (Supplemental Figure S6A). Thus, four additional MBP-TD2 C-terminal truncations within the last 94 amino acids were prepared (Supplemental Figure S6C) and analyzed for loss of detection by the α-pAdi3 antibody. In WB analysis, all four C-terminally truncated versions of TD2 were not detected by the α-pAdi3 antibody (Supplemental Figure S6D, lanes 3-6). These data indicate the TD2 epitope detected by the α-pAdi3 antibody must be located within the last 22 amino acids at the C-terminus of the protein. The  $\alpha$ -pAdi3 antibody is capable of detecting the phosphorylated Ser539 residue of Adi3 (Supplemental Figure S2). The last 22 amino acids contain a single Ser residue (Supplemental Figure S6C, Ser594), which could possibly be phosphorylated by an E. coli kinase for detection by the  $\alpha$ -pAdi3 antibody. To examine the possibility of an E. coli kinase-mediated phosphorylation event on this residue, Ser594 was mutated to Ala to inhibit any phosphorylation event that may occur when the protein is expressed in E. coli. Detection of the MBP-TD2<sup>S594A</sup> protein by the α-pAdi3 antibody was not eliminated (Figure 2E, lane 5), suggesting the α-pAdi3 antibody does not detect a phosphorylation event on the TD2 protein.

Since the  $\alpha$ -pAdi3 antibody was designed to detect a phosphorylation event on Adi3 (Figure 1A), the antibody may be detecting other negative charges within the last 22 amino acids of TD2. The terminal Glu595 has two negative charges; the carboxyl in the side chain and the free carboxyl termini. Therefore, to test whether the double negative charges on Glu595 could be a part of the TD2 epitope for the  $\alpha$ -pAdi3 antibody, several MBP-TD2 point mutants, removal of Glu595 (TD2 $^{\Delta E595}$ ), mutation to Ala (TD2 $^{E595A}$ ), and addition of Ala after Glu595 (TD2<sup>+Ala</sup>), were analyzed by WB with the  $\alpha$ -TD2 and  $\alpha$ -pAdi3 antibodies (Figure 2, D and E). Interestingly, all of these mutants showed loss of TD2 detection by the  $\alpha$ -pAdi3 antibody, but no loss of detection by the α-TD2 antibody (Figure 2, D and E, lanes 2-4), suggesting Glu595 is required for detection by the  $\alpha$ -pAdi3 antibody, and at a minimum the negative charge of a free carboxyl termini is required since the addition of an Ala residue after Glu595 (TD2+Ala) would eliminate this negative charge and is not detected by the  $\alpha$ -pAdi3 antibody (Figure 2E, lane 4). Moreover, in an effort to determine the precise  $\alpha$ -pAdi3 antibody epitope in TD2, the four residues located upstream of Glu595 were substituted to Ala individually and in combinations. Probably because the  $\alpha$ -TD2 antibody is polyclonal (Chen et al., 2007; Gonzales-Vigil et al., 2011), all MBP-TD2 versions were detected by the  $\alpha$ -TD2 antibody (Figure 2D, lanes 5–9). However, in the  $\alpha$ -pAdi3 WB, all double, triple, quadruple mutants showed reduced MBP-TD2 detection (Figure 2E, lanes 5–9) except the S594A mutant (Figure 2E, lane 5). Taken together, these data indicate Glu595 of TD2 is indispensable for TD2 detection by the  $\alpha$ -pAdi3 antibody, but several hydrophobic amino acids such as Leu591 and Val592/593 are required for full detection by the  $\alpha$ -pAdi3 antibody.

Interestingly, absolute conservation of a C-terminal Glu is observed in the TD2 sequences from plants belonging to the Solanaceous family, and not in the TD1 proteins (Supplemental Figure S7). The TD1 and TD2 protein sequences were obtained from 11 Solanaceous plants, plus from chickpea (Cicer arietinum) and the Arabidopsis thaliana TD sequence, and analyzed phylogenetically with the E. coli TD sequence used as an outlier (Supplemental Figure S7A). The analysis shows that the TD1 and TD2 sequences clearly cluster in separate groups (Supplemental Figure S7A). The TD2 sequences have a 100% conservation of a C-terminal Glu for all Solanaceous plants analyzed (Supplemental Figure S7, C and D). However, the TD1 sequences contain neither a carboxyl-Glu or any negatively charged amino acids within 7 amino acids from the C-terminus (Supplemental Figure S7B), which corresponds with the inability of the  $\alpha$ -pAdi3 antibody to detect TD1 (Figure 2B).

## Determination of the event occurring on TD2 in response to flg22 leading to loss of detection by the $\alpha$ -pAdi3 antibody

To identify the molecular event leading to reduced TD2 detection by the α-pAdi3 antibody, three different approaches were taken. First, the possibility of flg22-induced TD2 degradation was investigated. If TD2 degradation is involved, detection of TD2 by the polyclonal  $\alpha$ -TD2 antibody should also be reduced in response to flg22. However, when leaf protein extracts treated with or without the flg22 peptide were analyzed by WB, similar amounts of TD2 were detected by the  $\alpha$ -TD2 antibody in both samples (Figure 3A, left panels). But, TD2 detection by the α-pAdi3 antibody was compromised in response to a flg22 treatment (Figure 3A, right panels). Taken together, these data suggest TD2 is not degraded, but possibly modified at or near the C-terminus in a manner that directly or indirectly affects Glu595, or a modification similar to the Ala replacement that reduced detection in Figure 2E, for loss of detection by the  $\alpha$ -pAdi3 antibody.

Next, leaf protein extracts treated with or without flg22 were loaded onto two different 2D SDS-PAGE gels to be blotted with the  $\alpha$ -TD2 and  $\alpha$ -pAdi3 antibodies (Supplemental Figure S8A). Interestingly, in the WB analysis TD2 migrating in the range of pH 4 was detected by the  $\alpha$ -TD2 antibody predominantly in the flg22-treated sample (Supplemental Figure S8B, blue box), and this TD2 showed highly decreased detection by the  $\alpha$ -pAdi3 antibody (Supplemental Figure S8C, blue box). This indicates the TD2 migrating in this region could be the TD2 modified in response to flg22 treatment, which leads to a change in

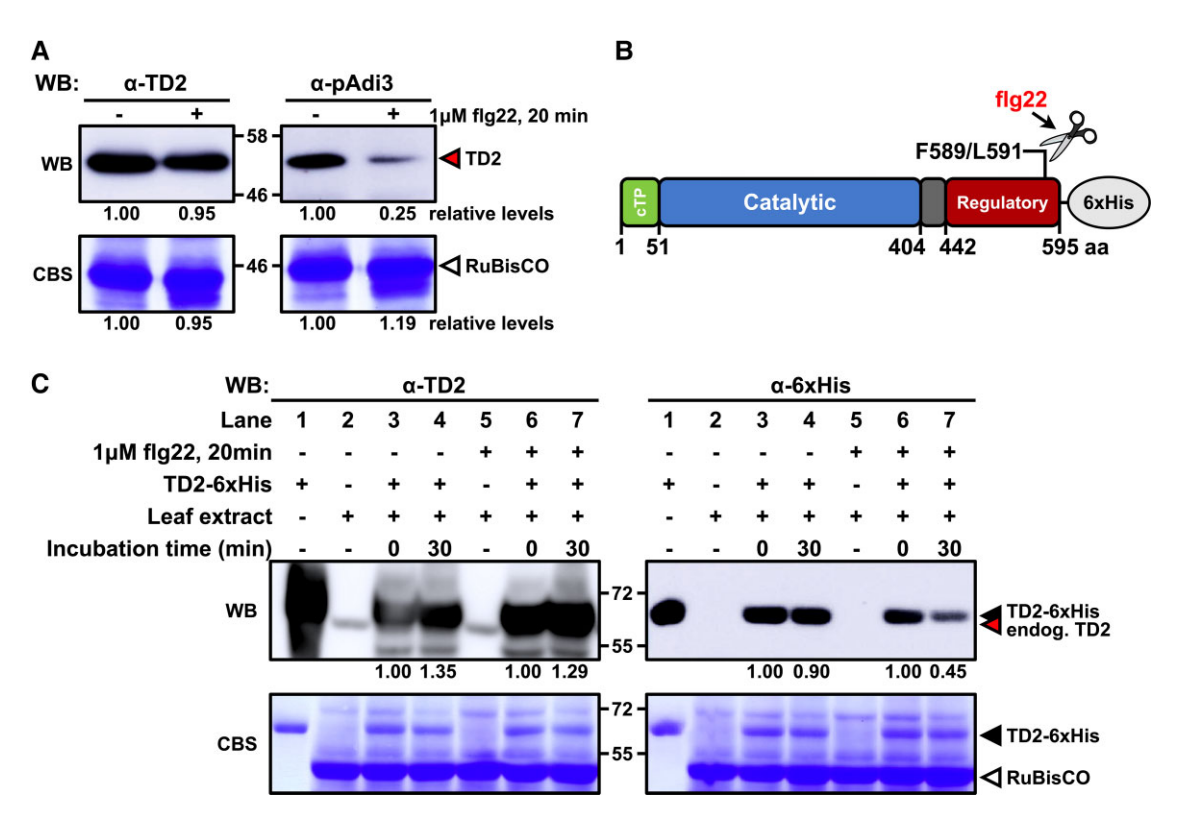


**Figure 3** flg22-induced proteolytic cleavage at the carboxyl-terminus of TD2. A, TD2 is not degraded in response to flg22. Tomato leaves were infiltrated with or without 1 μM flg22 for 20minutes, and 10 μg of a total protein leaf extract analyzed by  $\alpha$ -TD2 (left) or  $\alpha$ -pAdi3 (right) WB. B, Schematic diagram of TD2 domain structure. cTP indicates chloroplast transit peptide and position of possible flg22-induced F589 and L591 C-terminal cleavage sites identified by LC–MS/MS analysis is shown. C, Cell-free proteolytic cleavage of TD2. Recombinant TD2–6xHis protein shows a partial C-terminal cleavage in a flg22-dependent manner. Five hundred nanograms of TD2–6xHis was incubated for 0 or 30 minutes in the presence of 10 mM ATP with 10 μg of a soluble protein extract from tomato leaves infiltrated with or without 1 μM flg22 for 20 minutes. Samples were analyzed by  $\alpha$ -TD2 (left panel) and  $\alpha$ -6xHis (right panel) WB. TD2 detection levels were expressed relative to the detection of TD2 protein incubated with the protein extract for 0 minutes. In A and C, top panels, western blot (WB); bottom panels, Coomassie blue stain (CBS) of WB.

the acid/base properties of TD2. Three regions on the 2D gel showing detection of TD2 were excised for LC-MS/MS analysis (Supplemental Figure S8B, red boxes #1, #2 (pH 4 region), and #3). Unfortunately, very low TD2 peptide coverage was observed in all samples and peptides near the TD2 C-terminus were not detected in the pH 4 region sample where the modified TD2 is expected to be located (Supplemental Figure S8D).

Finally, the  $\alpha$ -TD2 antibody was covalently cross-linked to magnetic protein A beads (Supplemental Figure S9) for immunoprecipitation (IP) of the endogenous TD2 from flg22-treated leaf protein extracts followed by LC-MS/MS analysis. The MS analysis generated 92 peptides (Supplemental Data Set S1) for a 77% TD2 coverage and importantly, 7 peptides were found that covered the last 20 amino acids of the C-terminus (Supplemental Figure S10A). The C-terminal Glu595 is found in the tryptic peptide (K)LGYPYELDNYNEAFNLVVSE (Supplemental Figure S10A; Supplemental Data Set S1), however, no modifications to Glu595 were observed. Just upstream from Glu595, two C-terminally shortened peptides were identified, one peptide shortened by 6 amino acids and ending at Phe589, (K)LGYPYELDNYNEAF, (Supplemental Figure S10,

B and C; Supplemental Data Set S1) and one shortened by 4 amino acids ending at Leu591, (K)LGYPYELDNYNEAFNL (Supplemental Figure S10, D and E; Supplemental Data Set S1). These peptides were not considered as peptides hydrolyzed at the C-terminus by a posttreatment of trypsin because they were not cleaved at Arg or Lys residues (Olsen et al., 2004). Thus, the cleavage of these peptides at the C-terminus could have occurred in planta to the TD2 protein prior to extraction, or during sample processing. Furthermore, in planta C-terminal cleavage at Phe589 and/or Leu591 could be considered the potential flg22-induced TD2 modification because (1) these cleavage sites are located near the C-terminus (Figure 3B and Supplemental Figure S10); (2) removal of the TD2 amino acids after these cleavage sites should lead to a loss of TD2 detection by the  $\alpha$ -pAdi3 antibody; and (3) flg22 peptide treatment does not change the observed molecular weight of TD2 in WB analysis (Figure 3A), indicating that if TD2 is cleaved in response to flg22, only a few amino acids are removed from the C-terminus. To support these points, TD2 C-terminal truncations with all amino acids removed after Phe589 (MBP-TD2 $^{\Delta F589}$ ) or Leu591 (MBP-TD2<sup>ΔL591</sup>) displayed similar sizes on SDS-PAGE as

compared to MBP-TD2<sup>WT</sup>, and they were not detected by the  $\alpha$ -pAdi3 antibody as predicted because these truncations remove the epitope on TD2 for the  $\alpha$ -pAdi3 antibody (Supplemental Figure S11).

Next, to add support to the potential C-terminal cleavage event of TD2 in response to flg22 treatment, a cell-free cleavage assay was conducted with the 6xHis C-terminally tagged TD2 protein (TD2-6xHis). The TD2-6xHis protein was incubated for 0 or 30 minutes with extracts from leaves treated with or without the flg22 peptide. In this assay, if TD2-6xHis is C-terminally cleaved by a flg22-activated protease, TD2 should show a reduced detection by  $\alpha$ -6xHis WB due to loss of the 6xHis tag (Figure 3B), while  $\alpha$ -TD2 detection will be maintained. The results show that when TD2-6xHis was incubated for 30 minutes with a flg22-treated leaf extract, α-6xHis antibody detection of TD2-6xHis was reduced by 55% compared to the zero minute control (Figure 3C, right panel, compare lanes 6 and 7). This reduced TD2-6xHis detection was not induced by overall protein degradation because α-TD2-mediated detection was not decreased (Figure 3C, left panel, lanes 6 and 7). It should be noted the TD2-6xHis protein also displayed decreased detection by the α-6xHis antibody in the presence of a non-flg22-treated extract (Figure 3C, right panel, lanes 3 and 4). However, this reduced detection was 10% lower while the TD2-6xHis detection was reduced by 55% in the presence of the flg22-treated extract (Figure 3C, right panel, lanes 4 and 7). This assay was repeated with three additional biological replications with decreases in TD2-6xHis detection when incubated with flg22-treated extracts of 50%, 39%, and 22% (Supplemental Figure S12), and an N-terminally His-tagged TD2 (6xHis-TD2) did not show cleavage of the His tag in the presence of the flg22-treated extract (Supplemental Figure S13A) as compared to the C-terminally His-tagged TD2 (TD-6xHis) (Supplemental Figure S13B). Taken together, these data support our hypothesis that TD2 is C-terminally cleaved in response to flg22 treatment, possibly at Phe589 and/or Leu591 by a flg22-induced host protease. Additionally, the loss of TD2 detection in response to flg22 by the α-pAdi3 antibody as seen in Figure 1B is the result of the loss of the TD2 C-terminal residues by cleavage at Phe589/Leu591.

### C-terminal cleavage of TD2 alters its enzymatic activity

To understand how proteolytic cleavage at the carboxylterminus of TD2 affects its enzymatic properties, TD2 activity and Ile-feedback inhibition rates for the  $\mathrm{TD2}^{\Delta\mathrm{F589}}$  and  $\mathrm{TD2}^{\Delta\mathrm{L591}}$  mutants were measured and compared to WT TD2 (TD2<sup>WT</sup>). The  $\mathrm{TD2}^{\Delta\mathrm{F589}}$  and  $\mathrm{TD2}^{\Delta\mathrm{L591}}$  truncated proteins did not show different enzyme activity from  $\mathrm{TD2}^{\mathrm{WT}}$  (Figure 4A). In contrast, the two C-terminally truncated mutants were more sensitive to Ile-feedback inhibition, with  $\mathrm{TD2}^{\Delta\mathrm{L591}}$  having the highest sensitivity to Ile-feedback inhibition (Figure 4B). Interestingly, while  $\mathrm{TD2}^{\Delta\mathrm{F589}}$  was more inhibited than  $\mathrm{TD2}^{\mathrm{WT}}$ 

by Ile at levels below 1 mM, at Ile levels 1 mM or higher  $TD2^{\Delta F589}$  was inhibited at a rate similar to  $TD2^{WT}$  (Figure 4B).

Two allosteric effectors, Ile and valine (Val), differently regulate TD enzymatic properties during Ile biosynthesis (Supplemental Figure S1; Eisenstein et al., 1994). It has been shown that while Ile inhibits TD activity, this inhibition can be partially reversed by Val (Chen et al., 2013) (Supplemental Figure S1). Thus, the ability of Val to partially reverse the Ile-feedback inhibition of the TD2<sup>ΔF589</sup> and TD2<sup>ΔL591</sup> mutants was tested. Although TD2<sup>WT</sup> showed a 12% reduction in activity in the presence of Val alone, the presence of Val rescued the Ile inhibited TD2<sup>WT</sup> activity by 16% (Figure 4C). The Ile inhibited activity of the TD2<sup>ΔF589</sup> and TD2<sup>ΔL591</sup> mutants was not rescued by Val, and TD2<sup>ΔL591</sup> showed highly compromised activity in the presence of Val alone as compared to TD2<sup>WT</sup> and TD2<sup>ΔF589</sup> (Figure 4C).

Next, changes in endogenous TD2 enzymatic activity were measured in response to flg22. Previously studies have shown tomato TD2 to be heat resistant and exhibit maximal enzyme activity at 60°C, while TD1 activity is completely eliminated at 60°C with a maximum at 16°C (Gonzales-Vigil et al., 2011). Consequently, assessment of TD enzyme activity at 60°C will only measure activity from the TD2 protein. Thus, TD2 activity was tested at 60°C using soluble proteins extracted from tomato leaves treated with or without 1 µM flg22. The results show TD2 activity in the flg22-treated samples had a 64% decrease compared to the control (Figure 4D). Additionally, TD2 enzyme activity in the flg22-treated leaf protein extract was more sensitive to the Ile-feedback inhibition compared to the dH<sub>2</sub>O-treated sample (Figure 4E). Taken together, these data suggest the TD2 protein may be cleaved in response to flg22 and this modification compromises TD2 enzyme activity by increasing sensitivity to Ile.

It is possible that changes in the TD2 structure caused by truncation at Phe589 and/or Leu591 are responsible for the alterations seen in TD2 enzyme activity and Ile-feedback regulation in response to flg22. To analyze this possibility, predicted structures of the full-length TD2 (without cTP) and the Phe589 and Leu591 truncated proteins were produced using AlphaFold (Jumper et al., 2021). An overlay of these three structures (Supplemental Figure S14A) showed no obvious overall differences in the structures. However, the position of one of the potential residues for Ile binding for feedback regulation, Glu522, was displaced in the Phe589 and Leu591 truncated proteins in relation to the full-length structure (Supplemental Figure S14B). At this time it is unknown if this is related to the changes in TD2 activity seen in this study.

#### Production of a TD2 knockdown line

To aid studies on the role of TD2 in host defense responses, two KD lines, TD2 KD1 and TD2 KD2, were generated in the Rio Grande PtoR cultivar. The transgenic plants were generated using the pHANNIBAL vector (Wesley et al., 2001) to generate a TD2 hairpin RNA construct for RNA-mediated

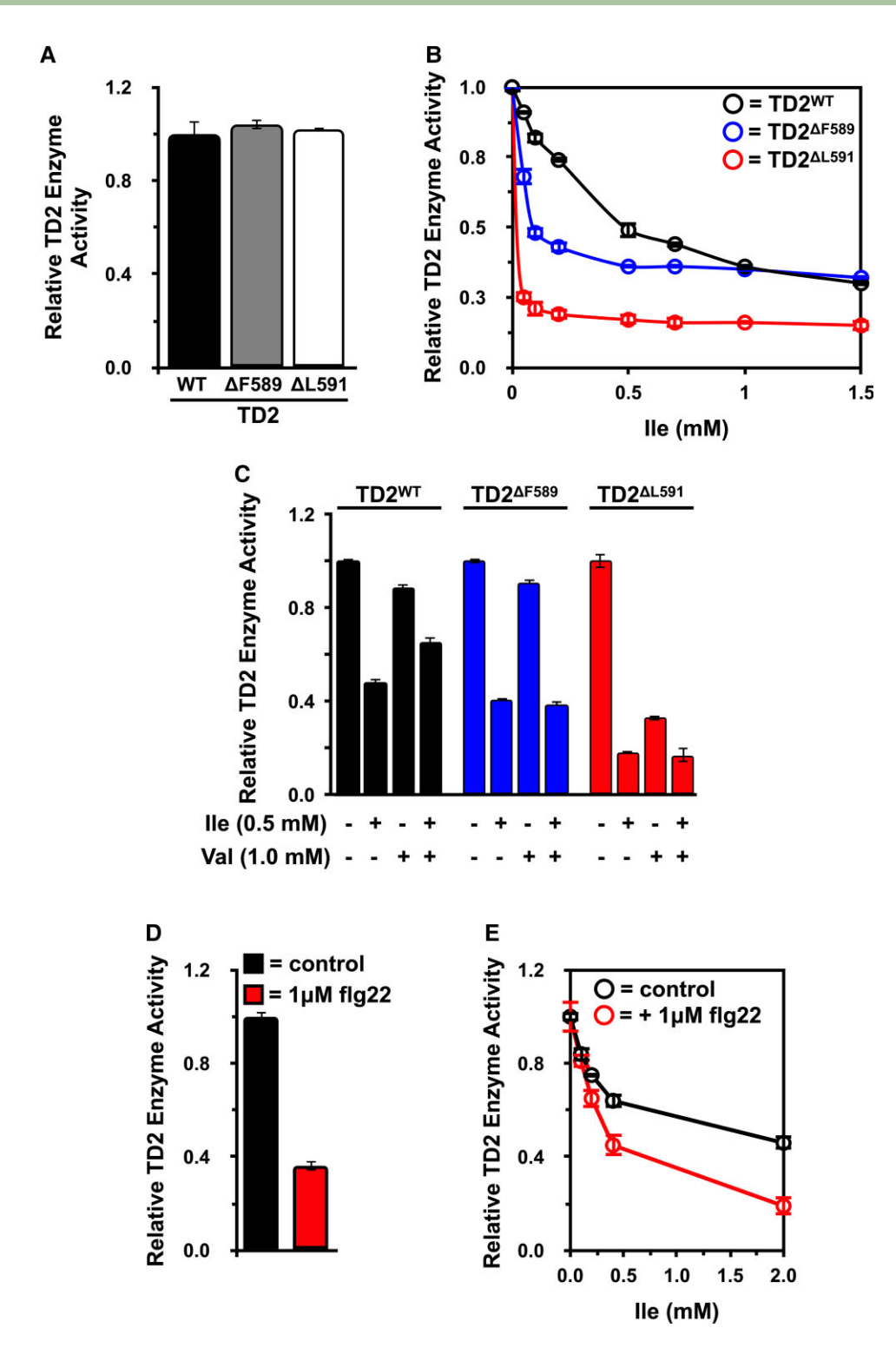


**Figure 4** Flg22 treatment induces changes in TD2 enzyme activity. A, Enzyme activity of wild-type (WT) TD2 and the C-terminally truncated TD2<sup>ΔF589</sup> and TD2<sup>ΔL591</sup> proteins. Fifty nanomoles of each MBP-TD2 protein was used to measure enzyme activity at room temperature for 30 minute. Error bars indicate standard error from three independent experiments. B, The C-terminally truncated TD2<sup>ΔF589</sup> and TD2<sup>ΔL591</sup> mutants display enhanced susceptibility to isoleucine (Ile)-mediated inhibition as compared to TD<sup>WT</sup>. Fifty nanomoles of each MBP-TD2 protein was used to measure enzyme activity at room temperature for 30 minutes in the absence or presence of 0.05, 0.1, 0.2, 0.5, 0.7, 1.0, and 1.5 mM Ile. C, Ability of Val to reverse lle inhibition of wild-type and C-terminally truncated TD2<sup>ΔF589</sup> and TD2<sup>ΔL591</sup> mutants. The indicated TD2 proteins were incubated at room temperature for 30 minutes in the presence of Ile and Val or in the presence of Ile plus Val at the indicated concentrations. D, Endogenous TD2 enzyme activity in response to flg22. Tomato leaves were infiltrated with dH<sub>2</sub>O or 1 μM flg22 for 20 minutes and TD2 activity from 10 μg of a soluble leaf protein extract was measured at 60°C for 30 minutes. E, Ile inhibition of endogenous TD2 in response to flg22. TD2 enzyme activity was tested with and without flg22 as in (D) plus in the presence of 0.1, 0.2, 0.4, and 2.0 mM Ile. In all panels, error bars indicate standard deviations from three independent experiments.

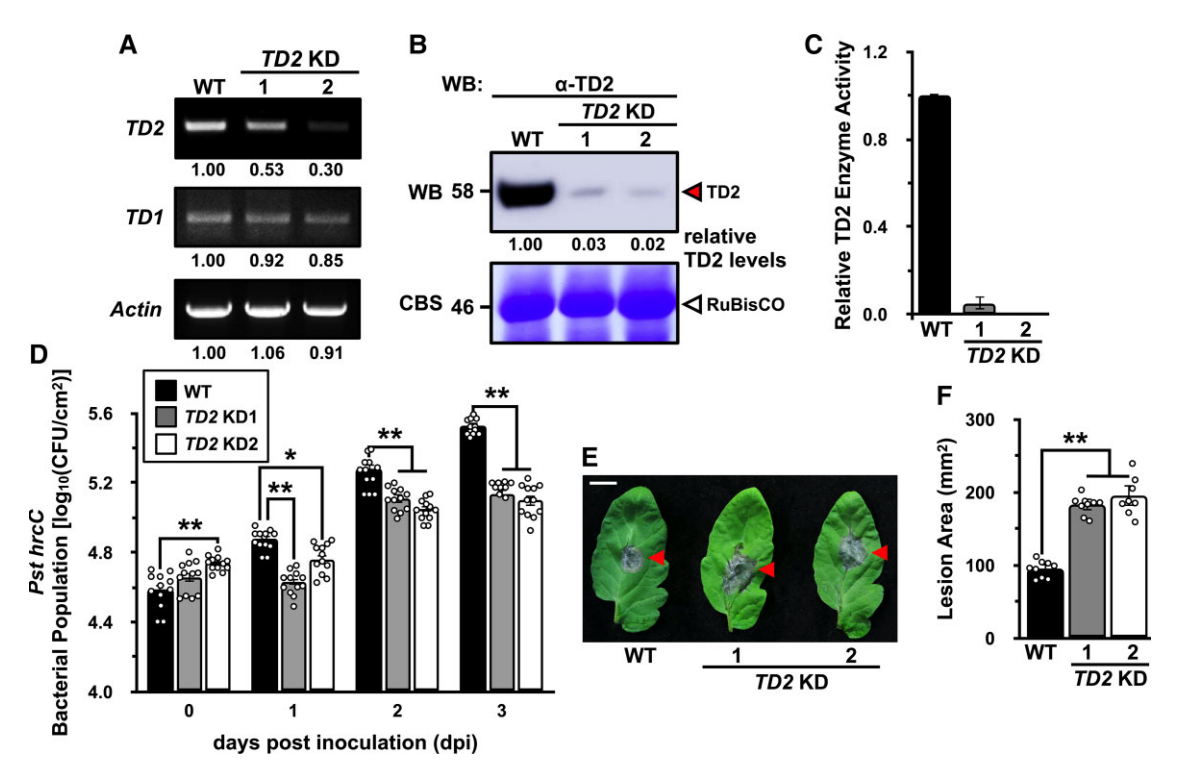


**Figure 5** Analysis of TD2 contributions to resistance against hemi/biotrophs and necrotrophs. A, Analysis of *TD1* and *TD2* mRNA levels in *TD2* KD plants. *TD1* and *TD2* mRNA were amplified by RT-PCR using cDNA from PtoR wild-type (WT) and *TD2* KD plants. Transcript levels are expressed relative to the level observed in the PtoR WT plants. B, Analysis of TD2 protein levels in *TD2* KD plants. The α-TD2 antibody was used in a western blot (WB) with 10 μg of soluble leaf protein extract to detect TD2 protein levels in PtoR WT and *TD2* KD plants. TD2 detection levels are expressed relative to the detection in the PtoR WT plants. Top panel, WB; bottom panel, Coomassie blue stain (CBS) of WB. C, Analysis of TD2 enzyme activity in *TD2* KD plants. TD2 activity was measured using 10 μg of a soluble leaf protein extract from the *TD2* KD plants at 60°C for 30 minutes. D, TD2 negatively regulates host defense against hemi/biotrophic infection. Five-week-old PtoR WT and *TD2* KD plants were vacuum-infiltrated with *Pst hrcC* at a density of 1 × 10<sup>6</sup> CFU/ml and bacterial leaf populations were measured at 0, 1, 2, and 3 days post-infection (dpi). Error bars indicate standard deviation from three independent experiments. E, TD2 positively regulates host defense against necrotrophic infection. Detached leaflets from the second and third leaf of 5-week-old PtoR WT and *TD2* KD plants were spotted with a 10-μl *B. cinerea* spore suspension (10<sup>6</sup> spores/ml). Photographs of the infected leaflets were taken 2 days after infection. Red arrows indicate necrotic lesions caused by *B. cinerea*, scale bar = 1 cm. Images are representative of three independent experiments. F, Quantification of the data in (E). The lesion areas in (E) were measured using ImageJ. Error bars represent standard error from three independent experiments. In D and F, asterisks indicate significant difference from WT according to one-way ANOVA, Tukey's multiple comparisons test: \*P < 0.005; \*\*P < 0.0001.

silencing (Supplemental Figure S15A). The region of TD2 used for the hairpin construct was a 275-bp region near the 5' end of the cDNA that was different from TD1 so as to not cause cross-silencing (Supplemental Figure S15B). RT-PCR analysis showed that the TD2 KD1 and KD2 plants have a reduction in TD2 expression levels as compared to the PtoR WT plant (Figure 5A). TD1 expression levels were largely unchanged in the TD2 KD plants (Figure 5A). Moreover, TD2 protein levels were also reduced in both KD plants as analyzed by  $\alpha$ -TD2 WB (Figure 5B), with a corresponding reduction in TD2 enzyme activity (Figure 5C).

### TD2 has opposite roles in host defense to hemibiotrophic and necrotrophic pathogens

To test whether the WT and TD2 KD plants show different levels of resistance to bacterial infection, PtoR WT and the two TD2 KD plants were infected with the Pst hrcC mutant and the level of leaf bacterial growth was analyzed every day

for 3 days (Figure 5D). The *Pst hrcC* mutant was used because it is unable to deliver effector proteins into plant cells (Yuan and He, 1996; Roine et al., 1997), and thus infection with *Pst hrcC* allows for measurement of PTI-mediated resistance only. At 1 day post-infection (1 dpi), both *TD2* KD plants showed significantly less bacterial growth, and thus more resistance to *Pst hrcC* compared to PtoR WT plants (Figure 5D). This higher resistance against *Pst hrcC* was maintained until 3 dpi in both KD plants (Figure 5D). These data indicate TD2 negatively contributes to the host immune response against bacterial hemibiotroph pathogen attack.

Next, in an effort to determine whether TD2 is also involved in the defense response to necrotrophic pathogens, *Botrytis cinerea* infection assays were performed using PtoR WT and TD2 KD plants. The infection assay showed that *B. cinerea* induced significantly larger lesions in both TD2 KD plants as compared to the PtoR WT plants (Figure 5, E and F), indicating that both

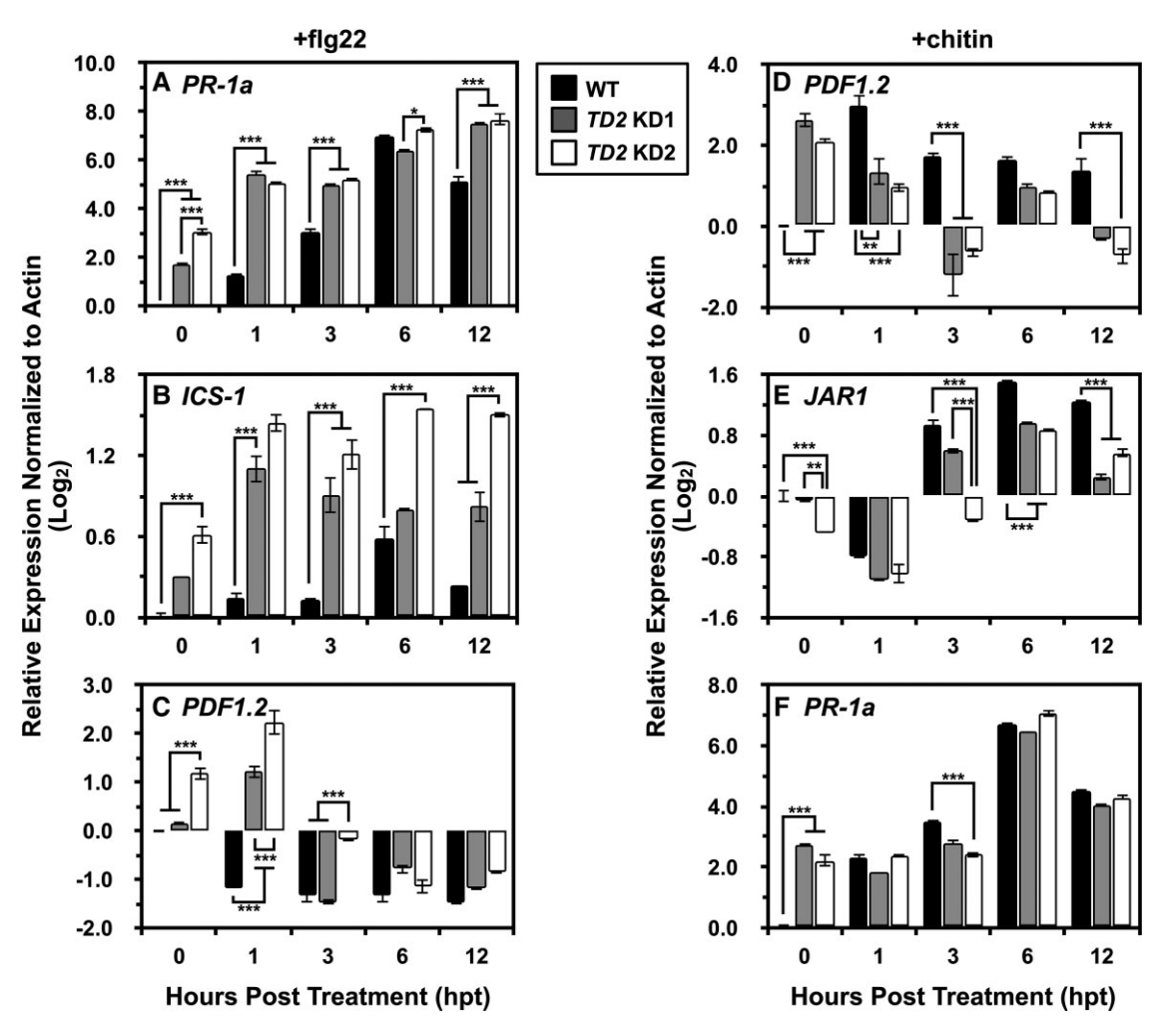


**Figure 6** TD2 effects on SA- and JA-responsive gene expression in response to hemi/biotroph and necrotroph PAMPs. Leaflets on the second leaf of 5-week-old PtoR wild-type and *TD2* KD plants were infiltrated with 1 μM flg22 (A–C) or 50 μg/ml chitin (D–F) to analyze expression levels of hormone-responsive genes by RT-qPCR. A–C, Expression of the SA-responsive genes *PR-1a* and *ICS-1* and the JA-responsive gene *PDF1.2* was analyzed in response to flg22. D–F, Expression of the JA-responsive genes *PDF1.2* and JAR1 and the SA-responsive gene *PR-1a* was analyzed in response to chitin. For all panels, expression levels were normalized to the expression of actin, error bars indicate standard deviation from three independent experiments, and asterisks indicate significant difference from WT according to one-way ANOVA, Tukey's multiple comparisons test: \**P* value between 0.01 and 0.001; \*\**P* value between 0.001 and 0.005; \*\*\*P value between 0.005 and 0.0001. JA, jasmonic acid, SA, salicylic acid, WT, wild-type.

KD plants are more susceptible to *B. cinerea* infection. Therefore, TD2 plays a positive functional role in the host defense against the necrotroph *B. cinerea*. Given the negative role TD2 has in PTI-based resistance to *Pst* (Figure 5D) and positive role in *B. cinerea* resistance (Figure 5, E and F), TD2 appears to act antagonistically in the interaction between hemibiotrophic and necrotrophic pathogens.

### TD2 effects on expression of SA and JA marker and biosynthesis genes in response to different PAMPs

Since our data indicate TD2 has an antagonistic function in host defense against hemibiotrophic and necrotrophic pathogens, and based on the known information on the antagonistic relationship between SA an JA in defense responses, it was investigated whether TD2 functions in the regulation of SA–JA crosstalk by analyzing gene expression

levels for SA and JA marker and biosynthesis genes in PAMP-treated *TD2* KD plants.

First, to determine the *TD2*-dependent SA-mediated gene expression changes in response to hemi/biotrophic pathogens, WT and *TD2* KD plants were treated with flg22 and gene expression changes were analyzed by RT-qPCR analysis. Expression levels for the SA-marker gene *pathogenesis-related protein 1* (*PR-1a*) (Ward et al., 1991; Takahashi et al., 2014), increased over the time course in all plants in response to flg22 (Figure 6A). However, the *TD2* KD plants showed a high basal expression level for *PR-1a* at 0 and 1 hour as compared to WT, and the *TD2* KD plants displayed a quicker and larger increase in *PR-1a* expression compared to PtoR WT over the 12-hour treatment (Figure 6A).

Additionally, a potential influence of TD2 on SA biosynthesis was analyzed by measuring alterations in *isochorismate* 

synthase-1 (ICS-1) expression, which is involved in SA hormone synthesis and has also been used as an SA-signaling marker gene (Wildermuth et al., 2001; Tsuda et al., 2008). Initial high expression levels of ICS-1 in response to flg22 were observed at the 0-, 1-, and 3-hour time points in TD2 KD plants and high ICS-1 expression levels were maintained over the 12-hour treatment as compared to WT (Figure 6B). Taken together, the increased expression levels of PR-1a and ICS-1 correspond with the increased resistance to Pst hrcC seen in the TD2 KD plants as compared to the PtoR WT plants (Figure 5D).

Next, the expression of the JA marker gene plant defensin 1.2 (PDF1.2) (Kachroo et al., 2003; Spoel et al., 2003; Lorenzo et al., 2004) was analyzed by RT-qPCR in WT and TD2 KD plants treated with flg22. Although the TD2 KD plants had higher initial PDF1.2 expression compared to WT, and the expression levels increased at the 1-hour time point, PDF1.2 expression levels quickly decreased and were not significantly different from WT plants at the 6- and 12-hour time points (Figure 6C). These results suggest that SA signaling is induced and JA signaling is compromised early in the TD2 KD plants in response to flg22. This combined with the bacterial resistance assays (Figure 5D) indicates that TD2 has a negative influence on the SA signaling pathway needed for host defense against hemibiotrophic pathogens.

In order to support the positive role of TD2 in host defense against necrotrophic fungi (Figure 5E, F), we analyzed the effect of TD2 on JA signaling and biosynthesis by monitoring gene expression changes by RT-qPCR in response to the fungal PAMP chitin (Doares et al., 1995a; Nojiri et al., 1996). The expression of PDF1.2 in WT plants quickly increased at the 1-hour time point, then gradually declined over the 12-hour time course, and was generally higher across all time points, except the 0 time point, compared to the TD2 KD plants (Figure 6D). In the TD2 KD plants, the basal PDF1.2 expression levels were high at the 0 time point, and then decreased to levels lower than WT over the 12-hour time course (Figure 6D). These results suggest JA signaling is compromised in the TD2 KD plants, which corresponds to the increased susceptibility seen in the B. cinerea infection assay (Figure 5, E and F).

The major bioactive form of the JA, JA–Ile, is generated by the conjugating enzyme jasmonyl-L-amino acid synthase 1 (JAR1) (Staswick et al., 2002; Suza and Staswick, 2008). The potential influence of *TD2* on JA biosynthesis was analyzed by measuring changes in *JAR1* gene expression in response to chitin. Although *JAR1* expression levels were generally decreased across all plants at the 1-hour time point, they increased in both wild-type and *TD2* KD plants over the rest of the 12-hour time course, with the WT expression higher than the *TD2* KD plants at 3, 6, and 12 hours (Figure 6E). This suggests production of JA–Ile is compromised in the *TD2* KD plants, which would lead to reduced resistance to necrotrophic pathogens. This agrees with our results from the *B. cinerea* infection assays (Figure 5, E and F).

Finally, the expression changes in the *PR-1a* SA marker were analyzed by RT-qPCR in WT and *TD2* KD plants treated with chitin. Although both *TD2* KD lines showed higher basal expression of *PR-1a* at the 0-hour time point, as was also seen in the flg22 treatment analysis (Figure 6A), PtoR WT and *TD2* KD lines did not show significantly different *PR-1a* expression levels after the 1-hour time point (Figure 6F). Interestingly, the expression levels of PR-1a were very similar in response to both flg22 and chitin at the 6-hour time point (Figure 6, A and F).

#### Discussion

The unexpected finding that TD2 has a negative function in host defense against bacterial hemibiotrophs

This study was initiated by the fortuitous discovery that TD2 can be detected by the  $\alpha$ -pAdi3 antibody, which was initially developed to detect the phosphorylated version of the Adi3 protein kinase (Figure 1A and Supplemental Figure S2), and the reduced detection of TD2 by this antibody in response to flg22 peptide treatment (Figure 1B). Based on the data presented, we propose a role for TD2 in host PTI early defense responses against bacterial infection. This is supported by the finding of enhanced resistance against Pst hrcC seen in the TD2 KD plants (Figure 5D), supporting a negative role for TD2 in the host defense response to bacterial pathogens. Accordingly, TD2 is functionally inhibited in response to flg22, presumably to reduce JA-IIe production and reduce interference with the SA signaling needed for full resistance to Pst. Interestingly, studies on the involvement of TD2 in the host immune response to bacterial pathogens have not been previously reported.

### Alterations in TD2 enzymatic properties in response to flg22

Through a combination of MS analysis (Supplemental Figure \$10) and the cell-free TD2 cleavage assay (Figure 3C), proteolytic cleavage at F589 and L591 near the C-terminus was identified as the possible modification of TD2 in response to flg22 treatment. Enzymatic analysis indicated that the truncated mutants  $TD2^{\Delta F589}$  and  $TD2^{\Delta L591}$  and the endogenous TD2 in response to flg22 treatment displayed enhanced sensitivity to Ile-feedback inhibition (Figure 4, B and E). This suggests that the endogenous TD2 is cleaved during the response to flg22. However, the recombinant TD2 $^{\Delta F589}$  and TD2 $^{\Delta L591}$  proteins did not have altered enzyme activity in the absence of Ile (Figure 4A), while the endogenous TD2 enzyme activity from flg22 treatment displayed a reduction of enzyme activity in the absence of Ile (Figure 4D). This contradiction in enzyme activity between  $TD2^{\Delta F589}/TD2^{\Delta L591}$  and endogenous TD2 in response to flg22 could be explained by other post-translational modifications (PTMs) to TD2. While we were able to identify several flg22-independent TD2 modifications by MS analysis

(Supplemental Figure S16), such as phosphorylation of Ser54 (Supplemental Figure S16, B and C) and deamination of several Gln (Supplemental Figure S16, D and E) and Asn (Supplemental Figure S16, F and G) residues, flg22-dependent PTMs were not identified. Additionally, recombinant TD2 was phosphorylated in a flg22-independent manner in an in vitro kinase assay using leaf soluble proteins (Supplemental Figure S17). Thus, future experiments should focus on identifying potential TD2 PTMs that may play a role in enzyme activity regulation in response to flg22.

The question of how C-terminal cleavage actually affects the enzymatic properties of TD2 remains to be determined. In terms of increased Ile sensitivity, it is possible cleavage causes a conformational change exposing a buried effector binding site or enhancing effector binding at the existing sites. Resolving this will require TD2 structural studies. Several past studies on E. coli TD (EcTD) and Arabidopsis thaliana TD (AtTD) have analyzed the TD structure in efforts to understand Ile allosteric regulation (Eisenstein, 1995; Gallagher et al., 1998; Halgand et al., 2002; Chen et al., 2013; Xing and Last, 2017). EcTD has been shown to have two Ile allosteric binding sites (Chen et al., 2013), each consisting of six amino acids (Supplemental Figure S18), while the two lle binding sites in AtTD involve two key Tyr residues; Tyr449 for the first site and Tyr 543 for the second site (Supplemental Figure S18; Wessel et al., 2000). However, any conformational changes caused by Ile, or the activator Val, are still elusive since the EcTD structure was determined in the absence of allosteric effectors. The crystal structure of tomato TD2 has been determined, however the protein used lacked the C-terminal regulatory domain (residues 78-415) (Gonzales-Vigil et al., 2011). Thus, this structure does not offer information about the effector inhibitory mechanism. To better understand the alteration of TD2 activity due to bacterial attack, the tomato TD2 protein structure containing both the catalytic and regulatory domains needs to be determined and compared in the absence or presence of allosteric effectors.

## Does tomato TD2 contribute to the regulation of SA–JA crosstalk during the plant response to hemibiotrophic bacterial attack?

In the pathogen infection assays, the *TD2* KD plants displayed opposite results for defense against pathogens with different pathogenic lifestyles (Figure 5, D and E). Because of the different strategies for these hemi/biotrophs and necrotrophs against plants, the host defenses will differentially control the pathogens via SA- or JA-mediated signaling pathways (Heil and Baldwin, 2002; Spoel et al., 2003; Bostock, 2005; Spoel et al., 2007; Caarls et al., 2015). For this reason, the two hormone signaling pathways cross-communicate in an antagonistic manner. For example, in plants that are resistant to hemi/biotrophs, JA-mediated signaling is suppressed by SA signaling in order to have maximal resistance (Doares et al., 1995b; Glazebrook, 2005; Spoel et al., 2007; Leon-Reyes et al., 2010).

In this study, the opposite roles of TD2 in defense against biotrophic and necrotrophic pathogens (Figure 5, D and E) suggest TD2 contributes to the crosstalk between SA and JA. This is supported by the finding that the TD2 KD lines treated with flg22 showed higher expression of the SA-responsive genes PR-1a and ICS-1 (Figure 6, A and B), but the JA-response genes PDF1.2 and JAR1 showed reduced expression in response to treatment with the necrotroph elicitor chitin, which stimulates JA-response signaling (Figure 6, D and E). To better understand the role of TD2 in SA-JA crosstalk, SA and JA hormone levels need to be measured and will be a focus of future studies.

However, there are several hurdles to overcome for future studies related to the role of TD2 in SA–JA crosstalk. Given that there are two TDs in tomato catalyzing the same reaction for Ile biosynthesis (Chen et al., 2007), a TD1/TD2 double mutant would need to be generated for future studies. However, this mutant is likely to be lethal or show severe developmental defects due to the essential function of TD in Ile production. In support of this, *N. attenuata* plants silenced for TD using a construct that targets both TD1 and TD2 were severely stunted (Kang et al., 2006).

Furthermore, it has been shown that the  $\alpha$ -ketobutyrate used for the biosynthesis of Ile can also be supplied from an alternative pathway in the cytoplasm where Met is converted to  $\alpha$ -ketobutyrate and methanethiol by methionine  $\gamma$ -lyase (MGL) (Joshi et al., 2010). This MGL-produced  $\alpha$ -ketobutyrate can be transported into the chloroplast for Ile biosynthesis (Joshi et al., 2010), indicating Ile equilibrium is maintained through the activity of TD and MGL. Thus, in TD2 KD plants, an analysis of MGL expression level changes and enzyme activity in response to flg22 or bacterial infection could be analyzed to better understand the role of TD2 in fine-tuning SA–JA crosstalk.

### A model for TD2 function in tomato defense against pst

Taken together, our data suggest a model (Figure 7A) for the role of TD2 in host-mediated defense against bacterial infection: (1) the C-terminus of TD2 is cleaved in response to bacterial attack, (2) the C-terminally cleaved TD2 activity is compromised via increased sensitivity to Ile-feedback inhibition, (3) this leads to lower levels of Ile for the JA–Ile conjugate, which leads to reduced activation of JA-mediated suppression of SA signaling, and (4) the host efficiently controls bacterial attack via increased activation of SA-mediated host defenses. Thus, TD2 has a negative role in hemi/biotroph resistance and a positive role in necrotrophy resistance (Figure 7B).

#### Materials and methods

### Plant growth conditions and generation of transgenic plants

The tomato (Solanum lycopersicum) cultivars Rio Grande, PtoR line, and MicroTom were used for the studies as

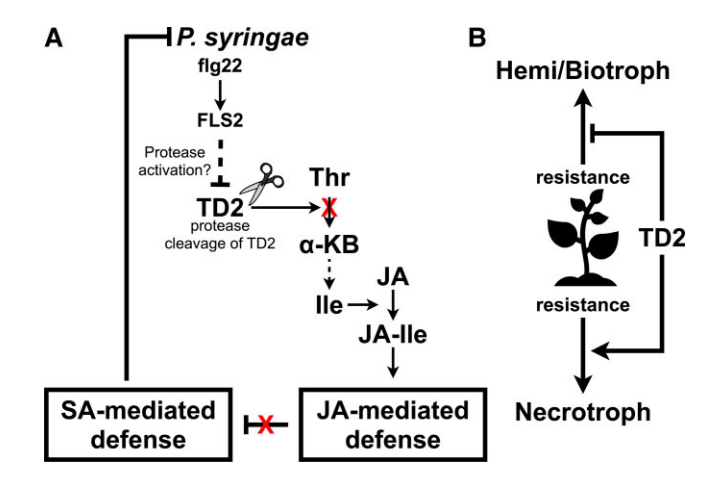


**Figure 7** Model for inhibition of TD2 during recognition of bacterial infection for reduction of JA–Ile production. A, Bacterial infection induces compromised activity of the host TD2 via C-terminal cleavage. Compromised TD2 activity leads to reduced production of JA–Ile, which results in diminished JA-mediated suppression of SA signaling. Consequently, SA-mediated host defenses contribute to full resistance to *Pst.* B, TD2 plays negative and positive roles in defense against hemi/biotrophic and necrotrophic pathogens, respectively. JA, jasmonic acid, SA, salicylic acid.

indicated. Plants were grown in a growth chamber maintained with a light intensity of  $150-200 \, \mu mole/m^2/sec$ , a 16-hour light period at 24°C followed by an 8-hour dark period at 20°C. A constant humidity of 70% was used.

### Cloning, site-directed mutagenesis, and recombinant protein expression and purification

All primers used in this study for ORF amplification, cloning, and site-directed mutagenesis are listed in Supplemental Table S1. The cDNAs of tomato TD1 (Solyc10g083760) and TD2 (Solyc09g008670.2.1) (Chen et al., 2007) were obtained by RT-PCR using tomato leaf total RNA isolated from leaflets of the second leaf of 5-week-old plants. The total RNA was extracted with TRIzol reagent (Life Technologies) and firststrand cDNA was generated with SuperScript III First-Strand Synthesis System (Invitrogen). The TD1 and TD2 ORFs were amplified by PCR from first strand cDNA with the primers listed in Supplemental Table S1 using Phusion High-Fidelity DNA Polymerase (ThermoFisher) and cloned into the BamHI and Sall sites of pMAL-c2x and the BamHI or EcoRI and Sall sites of pET-28a to express an N-terminal maltose binding protein (MBP) or a-6xHis translational fusion protein, respectively. Site-directed mutagenesis (SDM) was conducted on TD2 cloned into pMAL-c2x using Pfu Turbo DNA Polymerase (Stratagene) following manufacturer instructions using primers listed in Supplemental Table S1. Due to a BamHI site (nt 1,709–1,714) in TD1 that would prevent cloning into the BamHI of pMAL-c2x, this site was removed by SDM (GGATCC to GAATCC) without a change in the translated amino acid sequence. To clone the full-length TD2 cDNA into the EcoRI and Sall sites of pMAL-c2x, the EcoRI site in TD2 (nt 4–9) was removed by SDM (GAATTC to GAAATC) without a change in the translated amino acid sequence. The constructs were transformed into *E. coli* BL21 Star (DE3), grown at 37°C to OD<sub>600</sub> = 0.8, and protein expression induced by adding 100 μM isopropylthio- $\beta$ -D-galactoside (IPTG). The induced cultures were grown for an additional 16-hour at 18°C, and the expressed recombinant proteins were purified using amylose (NEB) or Ni-NTA agarose (QIAGEN) resins in a gravity-fed column for MBP or 6xHis translational fusing proteins, respectively.

### Flg22 treatments

Leaflets on the second or third leaves of 5-week-old plants were infiltrated with 1  $\mu$ M flg22 peptide dissolved in dH<sub>2</sub>O on the abaxial epidermis using a needleless syringe.

#### Western blot analysis

Proteins extracted from leaflet tissue (extracted in 50 mM Tris–HCl pH 8.0, 150 mM NaCl, 5 mM EDTA, 0.1% (v/v) Triton X-100, 1× protease inhibitor followed by centrifugation at 12,000×g, at 4°C for 10 minutes, and the supernatant was transferred to a clean tube) or purified from *E. coli* expression were separated by SDS–PAGE and detected by WB using a 1:2,000 dilution of the  $\alpha$ -TD2 antibody or a 1:200 dilution of the  $\alpha$ -pAdi3 antibody with a 1:3,000 dilution of an  $\alpha$ -rabbit-HRP antibody (ThermoFisher). WB detection was conducted using Amersham ECL prime western blot detection reagent (GE Healthcare) and the chemiluminescent signal was detected using an Amersham Imager 600 (GE Healthcare).

## Identification of TD2 as the protein detected by the $\alpha$ -pAdi3 antibody using 2D SDS-PAGE and mass spectrometry

Preparation of RuBisCO-depleted leaf protein extracts

For better separation of proteins during 2D SDS-PAGE analysis, the RuBisCO protein was depleted from the leaflet protein extracts following the protocol in (Krishnan and Natarajan, 2009). The tissue was ground in extraction buffer (50 mM Tris-HCl pH 8.0, 150 mM NaCl, 5 mM EDTA, 0.1% Triton X-100, 1× protease inhibitor cocktail) using a chilled dounce homogenizer, and soluble proteins were prepared by centrifugation at 125,000×g, at 4°C for 30 minutes and saving the supernatant (soluble extract). To deplete RuBisCO, 10 mM CaCl<sub>2</sub>·2H<sub>2</sub>O and 10 mM phytate were added to the soluble extract, samples incubated at 42°C for 10 minutes, the samples centrifugated at 12,000×g at room temperature for 10 minutes, and the supernatant transferred to a clean tube.

#### 2D SDS-PAGE and LC-MS/MS analysis

Two hundred micrograms of a RuBisCO-depleted leaf extract was loaded on each of two separate 2D SDS-PAGE gels with a first dimension pH range of 3-6 (Supplemental Figure S3, A and B). One gel was visualized by silver staining and the

second gel was transferred to a PVDF membrane for blotting with the  $\alpha$ -pAdi3 antibody (Supplemental Figure S3A). The two images of the stained gel and WB were overlaid in order to confirm the precise location(s) of the protein of interest on the silver-stained gel. The proteins on the silver-stained gel aligning with the WB (Supplemental Figure S3B) were excised for trypsin digestion followed by LC-MS/MS analysis to identify the protein. LC-MS/MS analysis was carried out at the University of Texas, San Antonio mass spectrometry core facility. The samples were reduced and alkylated with iodoacetamide prior to trypsin digestion, and mass spectra of trypsin-digested peptides were obtained using a ThermoFisher LTQ linear ion trap mass spectrometer with nano-LC peptide separations. MS/MS results were analyzed using Mascot (Matrix Science, London, UK; version 2.6.2) and X! Tandem (version CYCLONE). Mascot was set up to search the SwissProt 2017 02 database (553,655 entries) assuming trypsin digestion.

### Sequence alignment and phylogenetic analysis of TD proteins from solanaceous plants

The TD protein sequences shown in Supplemental Figure S19 were obtained from the Solanaceous Genomics Network (https://solgenomics.net), the Arabidopsis Information Resource (https://www.arabidopsis.org), Phytozome (https:// phytozome-next.jgi.doe.gov), and/or the NCBI GenBank database. Gene ID numbers and/or accession numbers for each TD sequence are given in Supplemental Figure S19. To analyze the phylogenetic relationship among these TD proteins, a multiple sequence alignment of the 22 TD protein sequences was generated using MUSCLE (MUltiple Sequence Comparison by Log-Expectation) (Edgar, 2004). A neighbor-joining phylogenetic tree was created from the aligned TD protein sequences using MEGA7 (Molecular Evolutionary Genetics Analysis) (Saitou and Nei, 1987; Kumar et al., 2016). To obtain the consensus sequence at the C-terminus of the TD proteins, the last 10 amino acids were analyzed using the online sequence logo generator WebLogo (Crooks et al., 2004).

# Isolation and analysis of endogenous TD2 for post-translational modification in response to flg22 Covalent cross-linking of the $\alpha$ -TD2 antibody to protein A beads

The  $\alpha$ -TD2 antibody was covalently cross-linked to protein A agarose beads to reduce the presence of antibody in the final sample, which can interfere with the analysis (Sisson and Castor, 1990). Protein A magnetic beads (New England Biolabs) were washed by resuspension in 100 mM sodium phosphate buffer pH 8.0, the beads pulled to the side of the tube with a magnet, and the supernatant removed. This step was repeated twice. Eighty microliters of 100 mM sodium phosphate buffer pH 8.0 was added to the washed protein A magnetic beads with 20  $\mu$ g of the  $\alpha$ -TD2 antibody, the sample mixed, and incubated at 4°C for 30 minutes with rotary shaking. The sample was then washed three times in

500 µl of 100 mM sodium phosphate buffer pH 8.0 as described above. Next, to covalently cross-link the antibody to protein A magnetic beads, 1 ml of cross-linking buffer (200 mM triethanolamine pH 8.2) was added to the antibody immobilized on the protein A magnetic beads, vortex to resuspend, the beads pulled to the side of the tube with a magnet, the supernatant removed, and the beads washed three times with cross-linking buffer as described above. Next, the sample was resuspended in 1 ml of cross-linking buffer with 25 mM dimethyl pimelimidate dihydrochloride (DMP) added (Supplemental Figure S9), mixed thoroughly, and incubated at room temperature for 45 minutes with rotary shaking. The beads were pulled to the side of the tube with a magnet, the supernatant removed, the sample resuspended in 1 ml of blocking buffer (100 mM ethanolamine pH 8.2), and the sample incubated at room temperature for 1 hour with rotary shacking. The antibody cross-linked protein A beads were washed three times in 1 ml 1x PBS buffer as described above. To remove any antibody that was not cross-linked, the antibody cross-linked protein A beads were resuspended in 1 ml elution buffer (100 mM glycine-HCl pH 2.5) and the supernatant removed. The beads were then resuspended in storage buffer (1x PBS, 0.1% Tween 20, 0.02% sodium azide) and stored at 4°C for future use.

### Isolation of the endogenous TD2 using the antibody cross-linked protein A beads

To isolate the endogenous TD2 protein using the  $\alpha$ -TD2 covalently cross-linked to the magnetic protein A beads, tomato leaflets form the second leaf of 5-week-old plants were infiltrated with 1 µM flg22 peptide, incubated for 20 minutes, protein extracted using extraction buffer (50 mM Tris-HCl pH 8.0, 150 mM NaCl, 5 mM EDTA, 0.1% Triton X-100, 1x protease inhibitor cocktail), the RuBisCO protein depleted from the extract as described above, and 100 µg of this extract incubated with the  $\alpha$ -TD2 cross-linked magnetic protein A beads in 1 ml IP buffer (20 mM Tris pH 7.5, 100 mM NaCl, 1 mM EDTA, 10% glycerol, 0.5% Triton X-100) at 4°C for 2 hours with agitation. After incubation, the beads were washed five times with 500 µl of IP wash buffer (20 mM Tris pH 7.5, 100 mM NaCl, 1 mM EDTA, 10% glycerol, 0.1% Triton X-100) using a magnet as described above. The TD2 protein bound to the  $\alpha$ -TD2 antibody cross-linked to the protein A resin was eluted by adding 50 µl of 5% SDS, pulling the beads to the side of the tube with a magnet, and collecting the supernatant. The IP was carried out five times in order to collect as much endogenous TD2 as possible. After the last IP all SDS elutions were pooled.

### Sample preparation for MS analysis

For MS analysis, the eluted native TD2 protein was digested by trypsin using the S-Trap system following manufacturer's instructions (ProtiFi). To reduce and alkylate disulfide bonds and cysteines, 20 mM DTT and 40 mM iodoacetamide were added to the eluate. The eluate was also acidified with 1.2% phosphoric acid and the acidified sample was resuspended in

S-Trap binding buffer [(90% methanol containing 100 mM triethylammonium bicarbonate (TEAB), pH 7.1]. The acidified eluate/S-Trap binding buffer mix was added into the spin column and centrifuged at  $4,000\times g$  for 1 minute. Next, the digestion buffer (50 mM TEAB, 20 µg trypsin) was added onto the column, centrifuged at  $4,000\times g$  for 1 minute, and incubated at  $47^{\circ}$ C for 2 hours. To elute the digested peptides from the column, digestion buffer without trypsin was added into the spin column and centrifuged at  $1,000\times g$  for 1 minute. To collect the hydrophobic peptides, 0.2% formic acid and 50% acetonitrile were added to the column and spun through at  $1,000\times g$  for 1 minute. All eluates were pooled and used for MS analysis.

#### Identification of the endogenous TD2 by LC-MS/MS analysis

LC-MS/MS analysis of the peptides was carried out at the University of Texas, San Antonio mass spectrometry core facility and results analyzed using Mascot and X! Tandem as described above. Carbamidomethyl of cysteine was specified in Mascot and X! Tandem as a fixed modification. Deamidation of asparagine and glutamine, oxidation of methionine, acetylation of the *N*-terminus, phosphorylation of serine, threonine and tyrosine and, and glutamylation of the C-terminus were specified in Mascot as variable modifications.

### Cell-free proteolytic cleavage assay

A cell-free cleavage assay was performed as previously described (Osterlund et al., 2000; Lee et al., 2008). In brief, leaflets from the second leaf of 5-week-old plants were infiltrated with or without 1  $\mu$ M flg22 for 20 minutes, extracts of the samples made using extraction buffer (25 mM Tris, pH 7.5, 10 mM MgCl<sub>2</sub>, 5 mM DTT, and 10 mM NaCl) with centrifugation at 12,000×g for 10 minute, and 10  $\mu$ g of the extracts with 10 mM ATP incubated in the absence or presence of 500 ng of recombinant TD2–6xHis protein at 30°C for 0 or 30 minutes. Reactions were stopped by the addition of 4× SDS–PAGE sample buffer, separated by 10% SDS–PAGE gels, and analyzed by WB using the  $\alpha$ -TD2 (at 1:2,000) and a-6xHis (at 1:2,000) antibodies.

### TD2 activity assay and feedback inhibition rate measurement

The TD2 enzyme activity assay is based on published protocols with minor modifications (Dougall, 1970; Mourad and King, 1995). In brief, 50 nM of the recombinant TD2 protein or 10  $\mu g$  of soluble leaf protein extract (50 mM Tris–HCl pH 8.0, 150 mM NaCl, 5 mM EDTA, 0.1% Triton X-100, 1× protease inhibitor cocktail) was incubated in 200  $\mu l$  of reaction buffer (100 mM potassium phosphate buffer pH 8.0, 20 mM L-threonine, and 1  $\mu M$  pyridoxal phosphate) at room temperature, 37°C, or 60°C for 30 minutes. To terminate the reaction and measure the generated  $\alpha$ -ketobutyric acid, 150  $\mu l$  of 30% trichloroacetic acid (w/v) and 200  $\mu l$  of 0.1% 2,4-dinitrophenylhydrazine in 1 N HCl were added and incubated at room temperature for 15 minutes. Finally, 400  $\mu l$  of

2.5 N KOH was added, mixed, and incubated at room temperature for 15 minutes. The amount of  $\alpha$ -ketobutyric acid produced was quantified via the ketone in  $\alpha$ -ketobutyric acid reacting with 2,4-dinitrophenylhydrazine, causing a color change measured by an absorbance reading at 515 nm using a spectrophotometer (BioMateTM3, ThermoFisher). To determine isoleucine feedback sensitivity of the TD2 protein, 20  $\mu$ l of different concentrations of isoleucine was added to 180  $\mu$ l of the TD2 reaction mix to give final Ile concentrations of 0.05, 0.1, 0.2, 0.5, 0.7, 1.0, and 1.5 mM, and TD2 activity was measured as described above. The relative TD2 activity was determined by the ratio between TD2 activities in the presence and absence of Ile.

### Generation of TD2 RNAi knockdown plants

Gene construct and Agrobacterium preparation

To silence the TD2 gene, a self-complementary hairpin RNA (hpRNA) construct containing sense/antisense arms with a PDK (pyruvate orthophosphate dikinase) intron as a loop structure (131 nt) was used (Supplemental Figure S15A). The TD2 nucleotides from 24 to 298 (Supplemental Figure S15B, 275 nt total) was used for the silencing construct. The sense and antisense nucleotides of that region were cloned into the multiple cloning sites upstream and downstream from the PDK intron of pHANNIBAL using the EcoRI and KpnI (sense) and HindIII and BamHI (antisense) sites (Supplemental Figure S15A). The TD2 hpRNA construct was transformed into Agrobacterium tumefaciens GV3101 by electroporation using a MicroPulser Electroporator following manufacturer's instructions (Bio-Rad). Transformed cells were grown at 30°C in 10 ml LB media with 50 μg/ml ampicillin and 25 µg/ml rifampicin overnight.

### Cotyledon explant generation and co-cultivation with Agrobacterium

Tomato Rio Grande PtoR seeds were sterilized with a mix of 70% ethanol and 20% bleach for 20 minutes and washed three times with sterile water. The sterilized seeds were germinated on Murashige and Skoog's (MS) medium under constant light at 24°C and 70% humidity. Once the cotyledons were fully expanded, approximately 8-day-old plants, they were cut from the plants, the tips cut, and three to four holes in the cotyledon were made using a sterile syringe needle in order to enhance infection opportunity and transformation efficiency for A. tumefaciens. The cotyledon explants were placed in MS plates media containing 30 mg/ml sucrose, 1 µg/ml 1-naphthaleneacetic acid (NAA), 1 µg/ml 6-benzylaminopurine (BAP) and pre-cultured for at room temperature for 24 hours under the constant light. An overnight Agrobacterium culture containing the TD2 hpRNA construct was adjusted to  $OD_{600} = 0.5$ , mixed with the cotyledon explants, and incubated at room temperature for 30 minutes. The cotyledons were removed from the bacterial suspension, placed on MS plates, and incubated at room temperature for 48 hours under constant light.

#### Regeneration and confirmation of TD2 gene silencing

The Agrobacterium-inoculated explants were maintained on MS plates containing 30 mg/ml sucrose, 1 µm/ml zeatin, 100 µm/ml ampicillin, and 300 µm/ml timentin to form callus tissue. Calli were transferred to fresh media plates every 2 weeks until shoots formed by somatic embryogenesis. Shoots were excised from the callus, placed in a magenta box containing MS media with 15 mg/ml sucrose, 1 µm/ml zeatin, 1 μm/ml gibberellic acid, 100 μm/ml ampicillin, and 300 µm/ml timentin, and grown under consistent light at RT until the shoot was approximately 5 cm. The shoots were excised from the calli and transferred to rooting media containing 15 mg/ml sucrose, 5 µm/ml indole-3-acetic acid, 100 μm/ml ampicillin, and 300 μm/ml timentin. Once plants were grown to about 5 cm with roots, they were transplanted to soil, covered with a magenta box to maintain high humidity, the cover removed after one week, and kept in a growth chamber at 24°C and 70% humidity on 18 hour light:6 hour dark cycle. Once plants were 2 weeks old, RNA was extracted from leaf tissue and silencing of the TD2 gene was confirmed by RT-PCR, RT-qPCR, and  $\alpha$ -TD2 WB analyses.

#### Pathogen resistance assays

#### Bacterial leaf growth assay

The test for resistance to the hemibiotrophic bacterial pathogen P. syringae pv. tomato used the bacterial leaf growth assay as previously described (Lin and Martin, 2005). In brief, the P. syringae pv. tomato (Pst) hrcC strain (Yuan and He, 1996; Tsuda et al., 2008) was cultivated overnight at 28°C in 10 ml King's B medium containing 50 μg/ml rifampicin. The bacteria were then harvested by centrifugation at 1,000×g at room temperature for 2 minutes, washed twice with sterilized dH<sub>2</sub>O, and resuspended in 1000 ml of 10 mM MgCl<sub>2</sub>. Three liters of 10 mM MgCl<sub>2</sub> with 0.002% Silwet was prepared and mixed with 3 ml of an  $OD_{600} = 1.0$ (10<sup>10</sup> CFU/ml) stock bacterial solution, which gave a final concentration of 10<sup>7</sup> CFU/ml. The bacterial solution was placed in a beaker inside a vacuum chamber, 5-week-old plants were inverted until fully submerged into the bacterial solution, the vacuum was applied to infiltrate the bacterial solution into the leaves, and after vacuum infiltration plants were incubated at 24°C under constant light. To monitor bacterial growth, six 0.635 cm diameter leaf discs were taken from terminal leaflets of the second or third leaves at 0, 1, 2, and 3 days after infiltration from three different plants for each time point. The 0 time point was collected approximately 15 minutes after bacterial infiltration. The disks were ground in 100 μl of 10 mM MgCl<sub>2</sub> with three zirconium oxide beads (2 mm diameter, Next Advance) using a Bullet Blender Storm 24 (Next Advance). Cell debris was removed by centrifugation at 800×g at room temperature for 1 min, and the supernatant was transferred to a clean tube. The samples were serially diluted and 10 µl of the dilutions were spotted on tryptone soya agar (Smolka et al., 2003) plates (1% Bacto tryptone, 1% sucrose, 0.1% glutamic acid,

and 1.5% agar) containing 25 µg/ml rifampicin, the plates incubated at 28°C, and bacterial CFUs were counted.

### Fungal leaf growth assay

To determine resistance against the necrotrophic fungal pathogen Botrytis cinerea previously published protocols were followed (Du et al., 2017). In brief, B. cinerea was cultured on V8 medium (10% V8 juice, 0.1% CaCO<sub>3%</sub> and 1.5% agar) at room temperature for one week. Conidia were collected and resuspended in liquid potato dextrose agar (PDA) medium (Bacto, USA) and the suspension passed through Miracloth. Six detached tomato leaflets from the second and third leaf of three different 5-week-old plants were spotted with a 10-µl spore suspension of 10<sup>6</sup> spores/ml. The infected leaflets were placed onto wet filter paper and incubated at room temperature in a culture box with a clear lid to maintain a moist environment. Pictures of the infected leaflets were taken at 2 days after inoculation and the necrotic halos were measured with ImageJ software using the polygon tool.

### RNA isolation and reverse transcription quantitative PCR (RT-qPCR)

To determine flg22- or chitin-induced changes in gene expression, leaflets from the second leaf of 5-week-old plants were treated with and without 1 μM flg22 or 50 μg/ml chitin by syringe infiltration for 0, 1, 3, 6, and 12 hours. RNA was extracted with TRIzol reagent (Life Technologies) and cDNA was generated by SuperScript<sup>TM</sup> III First-Strand Synthesis System (Invitrogen) according to the manufacturer's instructions. RT-qPCR was conducted with iTaq Universal SYBR Green Supermix (Bio-Rad) using a Bio-Rad CFX96 qPCR instrument (Bio-Rad) with primers listed in Supplemental Table S1. The thermal cycling program was 95°C for 30 seconds, 40 cycles of 95°C for 5 seconds and 60°C for 30 seconds. Actin was used as the internal reference. The relative C<sub>r</sub> (threshold cycle) values were measured and gene expression levels were measured using the 2 $^{-\Delta\Delta C}$  method (Livak and Schmittgen, 2001). Gene expression levels were normalized to actin expression levels. A cycle number of each gene was normalized to the cycle number of actin ( $\Delta C_t$ ) and the transformed cycle numbers ( $\Delta\Delta C_t$ ) were calculated and normalized to the  $\Delta C_t$  of each gene of the control plant.

#### In vitro kinase activity assay

In vitro kinase assays were performed in a total final volume of 30  $\mu$ l in a kinase buffer containing 10 mM Tris–HCl, pH 7.5, 150 mM NaCl, 10 mM MgCl<sub>2</sub>, and 1 mM DTT. Reactions including 3  $\mu$ g of recombinant TD2 and 10  $\mu$ g of soluble protein extract from leaves infiltrated with or without 1  $\mu$ M flg22 for 20 minutes were initiated with the addition of 1  $\mu$ Ci of [ $\gamma$ -<sup>32</sup>P]ATP (6,000 Ci/mmoL, Perkin-Elmer) and non-radiolabeled ATP to a final concentration of 20  $\mu$ M per reaction followed by incubation for 1 hour at RT. Reactions were stopped by the addition of 10  $\mu$ l 4× SDS–PAGE sample

buffer and samples separated on 8% SDS-PAGE gels. The proteins in the gels were visualized using GelCode Blue Stain Reagent (Thermo Fisher Scientific), and gels were dried and exposed overnight to a phosphor screen. Visualization and quantification of incorporated radioactivity were conducted using a phosphorimager (Typhoon FLA7000, GE Healthcare Life Sciences) and quantification software (ImageQuant TL, GE Healthcare Life Sciences).

#### **Accession numbers**

Sequence data from this article can be found in the GenBank/EMBL data libraries under accession numbers found in Supplemental Figure S19.

### Supplemental data

The following materials are available in the online version of this article.

**Supplemental Figure S1.** Threonine deaminase (TD) enzymatic reaction.

**Supplemental Figure S2.** Western blot (WB) detection of phosphorylated Adi3 using the  $\alpha$ -pAdi3 antibody to detect Ser539 phosphorylated Adi3.

**Supplemental Figure S3.** Identification of TD2 as the protein detected by the  $\alpha$ -pAdi3 antibody.

**Supplemental Figure S4.** Protein domain structure of tomato TDs and sequence alignment.

**Supplemental Figure S5.** Protein alignment of the MicroTom and PtoR Rio Grande TD2 sequences.

**Supplemental Figure S6.** Identification of the  $\alpha$ -pAdi3 antibody epitope in TD2.

**Supplemental Figure S7.** Phylogenetic analysis and conservation of C-terminal sequences for TD proteins from different plants.

**Supplemental Figure S8.** flg22-induced changes in TD2 detection by WB using  $\alpha$ -TD2 and  $\alpha$ -pAdi3 antibodies in 2D gel electrophoresis analysis.

**Supplemental Figure S9.** Production of an immobilized  $\alpha$ -TD2 antibody.

**Supplemental Figure S10.** Results of MS analysis on endogenous TD2 immunoprecipitated with the  $\alpha$ -TD2 antibody covalently cross-linked to magnetic protein A beads.

**Supplemental Figure S11.** Analysis of C-terminally truncated TD2<sup>ΔF589</sup> and TD2<sup>ΔL591</sup> by α-pAdi3 western blot.

**Supplemental Figure S12.** Biological replicates of cell-free flg22-induced proteolytic cleavage of TD2.

**Supplemental Figure S13.** flg22-induced TD2 cleavage is specific to the C-terminus.

**Supplemental Figure \$14.** Comparison of predicted protein structures between WT and C-terminal truncated versions of TD2.

**Supplemental Figure S15.** Design of a *TD2* knockdown construct.

**Supplemental Figure S16.** LC-MS/MS identification of endogenous post-translational modification (PTM) events on TD2.

**Supplemental Figure S17.** Identification of an flg22-independent phosphorylation event on TD2.

**Supplemental Figure \$18.** Alignment of TD proteins showing the allosteric binding sites.

**Supplemental Figure S19.** Protein sequences for all TD sequences used in this study for phylogenetic analysis.

Supplemental Table S1. Primers used in this study.

**Supplemental Dataset S1.** TD2 peptides identified after immunoprecipitation from flg22-treated leaf extracts.

### **Acknowledgments**

We thank Dr. Gregg A. Howe, Michigan State University, for generously providing the  $\alpha$ -TD2 antibody and seeds for the TD2 KD MicroTom line. We also thank Dr. Lawrence J. Dangott, Texas A&M Protein Chemistry Lab, for performing 2D SDS–PAGE analysis and helpful advice regarding MS analysis.

### **Funding**

This work was supported by the United States Department of Agriculture-National Institute of Food and Agriculture-Agriculture and Food Research Initiative grant #2014-67013-21560, National Science Foundation-Molecular and Cellular Biology-Systems and Synthetic Biology grant #1244068, and funds from the Texas A&M University Department of Biochemistry and Biophysics to T.P.D.

Conflict of interest statement. None declared.

#### References

Bergelson J, Dwyer G, Emerson JJ (2001) Models and data on plant-enemy coevolution. Annu Rev Genet 35(1): 469–499

**Bostock RM** (2005) Signal crosstalk and induced resistance: straddling the line between cost and benefit. Annu Rev Phytopathol **43**(1): 545–580

Butt A, Mousley C, Morris K, Beynon J, Can C, Holub E, Greenberg JT, Buchanan-Wollaston V (1998) Differential expression of a senescence-enhanced metallothionein gene in Arabidopsis in response to isolates of *Peronospora parasitica* and *Pseudomonas syringae*. Plant J **16**(2): 209–221

Caarls L, Pieterse CM, Van Wees SC (2015) How salicylic acid takes transcriptional control over jasmonic acid signaling. Front Plant Sci 6: 170

Chen H, Gonzales-Vigil E, Wilkerson CG, Howe GA (2007) Stability of plant defense proteins in the gut of insect herbivores. Plant Physiol 143(4): 1954–1967

Chen H, Wilkerson CG, Kuchar JA, Phinney BS, Howe GA (2005) Jasmonate-inducible plant enzymes degrade essential amino acids in the herbivore midgut. Proc Natl Acad Sci U S A 102(52): 19237–19242

Chen L, Chen Z, Zheng P, Sun J, Zeng AP (2013) Study and reengineering of the binding sites and allosteric regulation of biosynthetic threonine deaminase by isoleucine and valine in *Escherichia coli*. Appl Microbiol Biotechnol **97**(7): 2939–2949

Colmenares AJ, Aleu J, Duran-Patron R, Collado IG, Hernandez-Galan R (2002) The putative role of botrydial and related metabolites in the infection mechanism of *Botrytis cinerea*. J Chem Ecol **28**(5): 997–1005

- Crooks GE, Hon G, Chandonia JM, Brenner SE (2004) Weblogo: a sequence logo generator. Genome Res 14(6): 1188–1190
- Cui H, Tsuda K, Parker JE (2015) Effector-triggered immunity: from pathogen perception to robust defense. Annu Rev Plant Biol 66(1): 487–511
- **de Souza EM, Granada CE, Sperotto RA** (2016) Plant pathogens affecting the establishment of plant-symbiont interaction. Front Plant Sci **7**: 15
- Devarenne TP, Ekengren SK, Pedley KF, Martin GB (2006) Adi3 is a Pdk1-interacting AGC kinase that negatively regulates plant cell death. EMBO J 25(1): 255–265
- **Doares SH, Narvaez-Vasquez J, Conconi A, Ryan CA** (1995a) Salicylic acid inhibits synthesis of proteinase inhibitors in tomato leaves induced by systemin and jasmonic acid. Plant Physiol **108**(4): 1741–1746
- Doares SH, Syrovets T, Weiler EW, Ryan CA (1995b)
  Oligogalacturonides and chitosan activate plant defensive genes through the octadecanoid pathway. Proc Natl Acad Sci U S A 92(10): 4095–4098
- Dougall DK (1970) Threonine deaminase from Paul's scarlet rose tissue cultures. Phytochemistry **9**(5): 959–964
- Du M, Zhao J, Tzeng DTW, Liu Y, Deng L, Yang T, Zhai Q, Wu F, Huang Z, Zhou M, et al. (2017) MYC2 orchestrates a hierarchical transcriptional cascade that regulates jasmonate-mediated plant immunity in tomato. Plant Cell 29(8): 1883–1906
- Edgar RC (2004) MUSCLE: a multiple sequence alignment method with reduced time and space complexity. BMC Bioinform 5(1): 113
- Eisenstein E (1995) Allosteric regulation of biosynthetic threonine deaminase from *Escherichia coli*: effects of isoleucine and valine on active-site ligand binding and catalysis. Arch Biochem Biophys **316**(1): 311–318
- Eisenstein E, Yu HD, Schwarz FP (1994) Cooperative binding of the feedback modifiers isoleucine and valine to biosynthetic threonine deaminase from *Escherichia coli*. J Biol Chem **269**(47): 29423–29429
- Ek-Ramos MJ, Avila J, Cheng C, Martin GB, Devarenne TP (2010) The T-loop extension of the tomato protein kinase AvrPto-dependent pto-interacting protein 3 (Adi3) directs nuclear localization for suppression of plant cell death. J Biol Chem 285(23): 17584–17594
- Ek-Ramos MJ, Avila J, Nelson Dittrich AC, Su D, Gray JW, Devarenne TP (2014) The tomato cell death suppressor Adi3 is restricted to the endosomal system in response to the *Pseudomonas syringae* effector protein AvrPto. PLoS One **9**(10): e110807
- Faris JD, Friesen TL (2020) Plant genes hijacked by necrotrophic fungal pathogens. Curr Opin Plant Biol 56: 74–80
- Gallagher DT, Gilliland GL, Xiao G, Zondlo J, Fisher KE, Chinchilla D, Eisenstein E (1998) Structure and control of pyridoxal phosphate dependent allosteric threonine deaminase. Structure 6(4): 465–475
- **Glazebrook J** (2005) Contrasting mechanisms of defense against biotrophic and necrotrophic pathogens. Annu Rev Phytopathol **43**(1): 205–227
- Gonzales-Vigil E, Bianchetti CM, Phillips GN Jr, Howe GA (2011) Adaptive evolution of threonine deaminase in plant defense against insect herbivores. Proc Natl Acad Sci U S A 108(14): 5897–5902
- **Halgand F, Wessel PM, Laprevote O, Dumas R** (2002) Biochemical and mass spectrometric evidence for quaternary structure modifications of plant threonine deaminase induced by isoleucine. Biochemistry **41**(46): 13767–13773
- Heil M, Baldwin IT (2002) Fitness costs of induced resistance: emerging experimental support for a slippery concept. Trends Plant Sci 7(2): 61–67
- Jones JD, Dangl JL (2006) The plant immune system. Nature 444-(7117): 323–329
- Joshi V, Joung JG, Fei Z, Jander G (2010) Interdependence of threonine, methionine and isoleucine metabolism in plants: accumulation and transcriptional regulation under abiotic stress. Amino Acids 39(4): 933–947
- Jumper J, Evans R, Pritzel A, Green T, Figurnov M, Ronneberger O, Tunyasuvunakool K, Bates R, Zidek A, Potapenko A, et al. (2021)

- Highly accurate protein structure prediction with AlphaFold. Nature **596**(7873): 583–589
- Kachroo A, Lapchyk L, Fukushige H, Hildebrand D, Klessig D, Kachroo P (2003) Plastidial fatty acid signaling modulates salicylic acid- and jasmonic acid-mediated defense pathways in the Arabidopsis ssi2 mutant. Plant Cell 15(12): 2952–2965
- Kang JH, Wang L, Giri A, Baldwin IT (2006) Silencing threonine deaminase and JAR4 in Nicotiana attenuata impairs jasmonic acid-isoleucine-mediated defenses against Manduca sexta. Plant Cell 18(11): 3303–3320
- **Krishnan HB, Natarajan SS** (2009) A rapid method for depletion of rubisco from soybean (*Glycine max*) leaf for proteomic analysis of lower abundance proteins. Phytochemistry **70**(17–18): 1958–1964
- Kumar S, Stecher G, Tamura K (2016) MEGA7: molecular evolutionary genetics analysis version 7.0 for bigger datasets. Mol Biol Evol 33(7): 1870–1874
- Lee JH, Terzaghi W, Gusmaroli G, Charron JBF, Yoon HJ, Chen HD, He YJ, Xiong Y, Deng XW (2008) Characterization of Arabidopsis and rice DWD proteins and their roles as substrate receptors for CUL4-RING E3 ubiquitin ligases. Plant Cell 20(1): 152–167
- Leon-Reyes A, Van der Does D, De Lange ES, Delker C, Wasternack C, Van Wees SC, Ritsema T, Pieterse CM (2010) Salicylate-mediated suppression of jasmonate-responsive gene expression in Arabidopsis is targeted downstream of the jasmonate biosynthesis pathway. Planta 232(6): 1423–1432
- **Li B, Meng X, Shan L, He P** (2016) Transcriptional regulation of pattern-triggered immunity in plants. Cell Host Microbe **19**(5): 641–650
- Li N, Han X, Feng D, Yuan D, Huang LJ (2019) Signaling crosstalk between salicylic acid and ethylene/jasmonate in plant defense: do we understand what they are whispering? Int J Mol Sci 20(3): 671
- **Lin NC, Martin GB** (2005) An avrPto/avrPtoB mutant of *Pseudomonas* syringae pv. tomato DC3000 does not elicit Pto-mediated resistance and is less virulent on tomato. Mol Plant Microbe Interact **18**(1): 43–51
- Liu L, Sonbol FM, Huot B, Gu Y, Withers J, Mwimba M, Yao J, He SY, Dong X (2016) Salicylic acid receptors activate jasmonic acid signal-ling through a non-canonical pathway to promote effector-triggered immunity. Nat Commun 7(1): 13099
- **Livak KJ, Schmittgen TD** (2001) Analysis of relative gene expression data using real-time quantitative PCR and the  $2-\Delta\Delta$ CT method. Methods **25**(4): 402–408
- Lorenzo O, Chico JM, Sanchez-Serrano JJ, Solano R (2004) JASMONATE-INSENSITIVE1 encodes a MYC transcription factor essential to discriminate between different jasmonate-regulated defense responses in Arabidopsis. Plant Cell 16(7): 1938–1950
- Macho AP, Zipfel C (2014) Plant PRRs and the activation of innate immune signaling. Mol Cell **54**(2): 263–272
- MacKinnon SL, Keifer P, Ayer WA (1999) Components from the phytotoxic extract of *Alternaria brassicicola*, a black spot pathogen of canola. Phytochemistry **51**(2): 215–221
- Monod J, Wyman J, Changeux JP (1965) On the nature of allosteric transitions: a plausible model. J Mol Biol 12(1): 88–118
- Mourad G, King J (1995) L-O-Methylthreonine-resistant mutant of Arabidopsis defective in isoleucine feedback regulation. Plant Physiol **107**(1): 43–52
- Mur LA, Kenton P, Atzorn R, Miersch O, Wasternack C (2006) The outcomes of concentration-specific interactions between salicylate and jasmonate signaling include synergy, antagonism, and oxidative stress leading to cell death. Plant Physiol 140(1): 249–262
- Nojiri H, Sugimori M, Yamane H, Nishimura Y, Yamada A, Shibuya N, Kodama O, Murofushi N, Omori T (1996) Involvement of jasmonic acid in elicitor-induced phytoalexin production in suspension-cultured rice cells. Plant Physiol 110(2): 387–392
- Olsen JV, Ong SE, Mann M (2004) Trypsin cleaves exclusively C-terminal to arginine and lysine residues. Mol Cell Proteomics **3**(6): 608–614

- Osterlund MT, Hardtke CS, Wei N, Deng XW (2000) Targeted destabilization of HY5 during light-regulated development of Arabidopsis. Nature 405(6785): 462-466
- Otani H. Kohnobe A. Kodama M. Kohmoto K (1998) Production of a host-specific toxin by germinating spores of Alternaria brassicicola. Physiol Mol Plant Pathol 52(5): 285-295
- Pieterse CM, Van der Does D, Zamioudis C, Leon-Reyes A, Van Wees SC (2012) Hormonal modulation of plant immunity. Annu Rev Cell Dev Biol 28(1): 489-521
- Reuber TL, Plotnikova JM, Dewdney J, Rogers EE, Wood W, Ausubel FM (1998) Correlation of defense gene induction defects with powdery mildew susceptibility in Arabidopsis enhanced disease susceptibility mutants. Plant J 16(4): 473-485
- Robert-Seilaniantz A, Grant M, Jones JD (2011) Hormone crosstalk in plant disease and defense: more than just jasmonate-salicylate antagonism. Annu Rev Phytopathol 49(1): 317-343
- Roine E, Wei W, Yuan J, Nurmiaho-Lassila EL, Kalkkinen N, Romantschuk M, He SY (1997) Hrp pilus: an hrp-dependent bacterial surface appendage produced by Pseudomonas syringae pv. tomato DC3000. Proc Natl Acad Sci U S A 94(7): 3459-3464
- Saitou N, Nei M (1987) The neighbor-joining method: a new method for reconstructing phylogenetic trees. Mol Biol Evol 4(4): 406-425
- Schenk PM, Kazan K, Wilson I, Anderson JP, Richmond T, Somerville SC, Manners JM (2000) Coordinated plant defense responses in Arabidopsis revealed by microarray analysis. Proc Natl Acad Sci U S A 97(21): 11655-11660
- Sidorov V, Menczel L, Maliga P (1981) Isoleucine-requiring Nicotiana plant deficient in threonine deaminase. Nature 294(5836): 87-88
- Sisson TH. Castor CW (1990) An improved method for immobilizing IgG antibodies on protein A-agarose. J Immunol Methods 127(2):
- Smolka B, Lukac R, Plataniotis KN, Venetsanopoulos AN (2003) Application of kernel density estimation for color image filtering, Proceedings of SPIE—The International Society for Optical Engineering, Vol. 5150: 1650-1656
- Spanu PD, Panstruga R (2017) Editorial: biotrophic plant-microbe interactions. Front Plant Sci 8: 192
- Spoel SH, Johnson JS, Dong X (2007) Regulation of tradeoffs between plant defenses against pathogens with different lifestyles. Proc Natl Acad Sci U S A 104(47): 18842-18847
- Spoel SH, Koornneef A, Claessens SM, Korzelius JP, Van Pelt JA, Mueller MJ, Buchala AJ, Metraux JP, Brown R, Kazan K, et al. (2003) NPR1 modulates cross-talk between salicylate- and jasmonate-dependent defense pathways through a novel function in the cytosol. Plant Cell 15(3): 760-770
- Staswick PE, Tiryaki I, Rowe ML (2002) Jasmonate response locus JAR1 and several related Arabidopsis genes encode enzymes of the firefly luciferase superfamily that show activity on jasmonic, salicylic, and indole-3acetic acids in an assay for adenylation. Plant Cell 14(6): 1405-1415
- Suza WP, Staswick PE (2008) The role of JAR1 in Jasmonoyl-L: -isoleucine production during Arabidopsis wound response. Planta 227(6): 1221-1232
- Takahashi H, Nakaho K, Ishihara T, Ando S, Wada T, Kanayama Y, Asano S, Yoshida S, Tsushima S, Hyakumachi M (2014) Transcriptional profile of tomato roots exhibiting Bacillus

- thuringiensis-induced resistance to Ralstonia solanacearum. Plant Cell Rep **33**(1): 99–110
- Thaler JS, Humphrey PT, Whiteman NK (2012) Evolution of jasmonate and salicylate signal crosstalk. Trends Plant Sci 17(5): 260-270
- Thaler JS, Owen B, Higgins VJ (2004) The role of the jasmonate response in plant susceptibility to diverse pathogens with a range of lifestyles. Plant Physiol 135(1): 530-538
- Thomma B, Eggermont K, Penninckx I, Mauch-Mani B, Vogelsang R, Cammue BPA, Broekaert WF (1998) Separate jasmonatedependent and salicylate-dependent defense-response pathways in arabidopsis are essential for resistance to distinct microbial pathogens. Proc Natl Acad Sci U S A 95(25): 15107-15111
- Truman W, Bennett MH, Kubigsteltig I, Turnbull C, Grant M (2007) Arabidopsis systemic immunity uses conserved defense signaling pathways and is mediated by jasmonates. Proc Natl Acad Sci U S A 104(3): 1075-1080
- Tsuda K, Sato M, Glazebrook J, Cohen JD, Katagiri F (2008) Interplay between MAMP-triggered and SA-mediated defense responses. Plant J **55**(5): 1061-1061
- Umbarger HE (1956) Evidence for a negative-feedback mechanism in the biosynthesis of isoleucine. Science 123(3202): 848
- van Wees SC, de Swart EA, van Pelt JA, van Loon LC, Pieterse CM (2000) Enhancement of induced disease resistance by simultaneous activation of salicylate- and jasmonate-dependent defense pathways in Arabidopsis thaliana. Proc Natl Acad Sci U S A 97(15): 8711-8716
- Vogel J, Somerville S (2000) Isolation and characterization of powdery mildew-resistant Arabidopsis mutants. Proc Natl Acad Sci U S A 97(4): 1897-1902
- Ward ER, Uknes SJ, Williams SC, Dincher SS, Wiederhold DL, Alexander DC, Ahl-Goy P, Metraux JP, Ryals JA (1991) Coordinate gene activity in response to agents that induce systemic acquired resistance. Plant Cell 3(10): 1085-1094
- Wesley SV, Helliwell CA, Smith NA, Wang MB, Rouse DT, Liu Q, Gooding PS, Singh SP, Abbott D, Stoutjesdijk PA, et al. (2001) Construct design for efficient, effective and high-throughput gene silencing in plants. Plant J 27(6): 581-590
- Wessel PM, Graciet E, Douce R, Dumas R (2000) Evidence for two distinct effector-binding sites in threonine deaminase by site-directed mutagenesis, kinetic, and binding experiments. Biochemistry 39(49): 15136-15143
- Wildermuth MC, Dewdney J, Wu G, Ausubel FM (2001) Isochorismate synthase is required to synthesize salicylic acid for plant defence. Nature 414(6863): 562-565
- Xing A, Last RL (2017) A regulatory hierarchy of the Arabidopsis branched-chain amino acid metabolic network. Plant Cell 29(6): 1480-1499
- Yang J, Duan G, Li C, Liu L, Han G, Zhang Y, Wang C (2019) The crosstalks between jasmonic acid and other plant hormone signaling highlight the involvement of jasmonic acid as a core component in plant response to biotic and abiotic stresses. Front Plant Sci 10: 1349
- Yuan J, He SY (1996) The Pseudomonas syringae Hrp regulation and secretion system controls the production and secretion of multiple extracellular proteins. J Bacteriol 178(21): 6399-6402
- Zipfel C (2014) Plant pattern-recognition receptors. Trends Immunol **35**(7): 345–351